2021-05-18

Sub- and Supercritical Water Gasification of Rice Husk: Parametric Optimization Using the I-Optimality Criterion.

Bakari, Ramadhani

ACS Publications

Article

Sub- and Supercritical Water Gasification of Rice Husk: Parametric Optimization Using the I-Optimality Criterion

Ramadhani Bakari,* Thomas Kivevele, Xiao Huang, and Yusufu A. C. Jande*
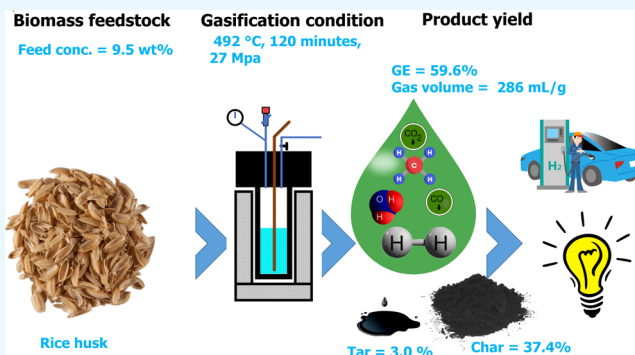
Cite This: *ACS Omega* 2021, 6, 12480−12499

Read Online

ACCESS | Metrics & More | Article Recommendations

ABSTRACT: In this study, rice husk biomass was gasified under sub- and supercritical water conditions in an autoclave reactor. The effect of temperature (350−500 °C), residence time (30−120 min), and feed concentration (3−10 wt %) was experimentally studied using the response surface methodology in relation to the yield of gasification products. The quadratic models have been suggested for both responses. Based on the models, the quantitative relationship between various operational conditions and the responses will reliably forecast the experimental outcomes. The findings revealed that higher temperatures, longer residence times, and lower feed concentrations favored high gas yields. The lowest tar yield obtained was 2.98 wt %, while the highest gasification efficiency and gas volume attained were 64.27% and 423 mL/g, respectively. The ANOVA test showed that the order of the effects of the factors on all responses except gravimetric tar yield follows temperature > feed concentration > residence time. The gravimetric tar yield followed a different trend: temperature > residence time > feed concentration. The results revealed that SCW gasification could provide an effective mechanism for transforming the energy content of RH into a substantial fuel product.

Biomass feedstock — Feed conc. = 9.5 wt%; Rice husk

Gasification condition — 492 °C, 120 minutes, 27 Mpa

Product yield — GE = 59.6%; Gas volume = 286 mL/g; Tar = 3.0 %; Char = 37.4%

1. INTRODUCTION

Biomass is a green fuel that is readily available globally, potentially accounting for 14−15% of overall energy consumption.[1] Biomass is also a cleaner fuel characterized by reduced sulfur, nitrogen, and carbon dioxide emissions.[2] In addition, it is of low cost and readily available in different forms, including agricultural residuals, wood, and energy crops. Rice is the second largest cultivated crop which produces a significant quantity of residuals globally. It is estimated that more than 150 million tons of rice husk (RH) are produced annually.[3,4] The literature shows that less than 17% of the RH is effectively utilized, and the remaining portion is disposed to the environment or directly burned, contributing to significant greenhouse emissions.[5−8] Reports on RH composition in the literature vary with hemicellulose typically of 11−29%, cellulose 31−44%, lignin 10−34%, ash 15−29%, and other extractive compounds.[9]

Supercritical water (SCW) gasification is a novel and effective thermochemical method to convert biomass into syngas—a hydrogen-rich gas with a stable fuel content like fossils. Besides, it features high reaction efficiency and H_2 selectivity among nearly any type of biomass, with no restriction on moisture content like in the classical gasification process.[10,11] SCW gasification, in fact, is considered the most cost-effective thermochemical conversion technology to convert biomass into hydrogen.[12] Most of the studies carried out on SCW gasification involved the use of biomass model compounds,[13] including cellulose,[14−18] lignin,[14,19,20] starch,[15] fructose,[21,22] and glycerol.[23,24] The use of model biomass provides a better understanding of the reaction mechanisms undergoing in the SCW gasification process. However, lignocellulosic compounds in real biomass undergo complex interaction reactions during gasification that cannot be apprehended with model biomass. Up to date, only a few studies have reported findings with real biomass.[25] The few available studies includes SCW gasification of sugarcane bagasse,[26,27] cornstalk,[1] food waste,[28] mosambi peels,[27] eucalyptus chips,[29] rice straw,[30] and RH.[31] Therefore, more research on real biomass is indispensable to understand their decomposition behavior in SCW conditions and anticipate the challenges in large-scale operations.[13]

Operating and design factors directly affect the SCW gasification performance, this includes the reaction temperature, reaction pressure, feed concentration, residence time, feed flow rate, type of reactor, reactor material, and catalyst, among others.
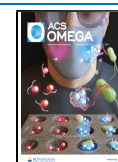
The optimization of these factors can significantly improve gasification efficiency (GE), thereby providing higher gas yield.[32] Some researchers have previously studied SCW gasification parameters; these include: (i) SCW gasification of eucalyptus chips at temperatures between 400 and 500 °C, pressures ranging from 20−22, 22−25 to 25−30 MPa, and various residence time (30, 45, or 60 min);[29] (ii) examination of the gasification mechanism of cornstalk in SCW at temperatures between 500−800 °C, residence time between 1 and 15 min, and feed concentration of 1−9 wt %;[1] (iii) production of H_2-rich gas from gasification of unsorted food waste in SCW at temperatures between 420 and 480 °C, residence time of 30−75 min, and feed concentration of 5−15 wt %; (iv) investigation of in situ SCW gasification of sugarcane bagasse at different temperatures (300, 350, 400, 450, and 500), biomass ratios (0.125, 0.167, 0.25, and 0.5), and a constant residence time of 50 min;[27] and finally (v) gasification of RH in SCW at temperatures between 400 and 680 °C, a biomass concentration between 2 and 14 wt %, a biomass particle size ranging from 250 to 1500 μm and a constant residence time of 1 h.

The above-mentioned studies have shown that the severity factors affecting the SCW gasification process are temperature, feedstock concentration, residence time, and pressure. Unfortunately, these reported studies used a classic one-factor-at-a-time (OFAT) experiment approach, which varies only one variable at a time while the other factors were held constant. Using this method, it is challenging to identify the optimum combination of the operating parameters, which requires a function expression between the factors and responses that can predict the gasification results. As contrasted to the OFAT method, the statistically designed experiments that vary many factors concomitantly and prudently are more effectual when studying the effect of more than one parameter because they include interaction(s) among factors.[33] The response surface methodology (RSM) is a combination of mathematical and statistical methods that can be used for studying the influence of several parameters at a different level, and hence, their impact on each other, overcoming the limitation of the classic OFAT method. Moreover, the RSM is advantageous in reducing the number of experiments, cost, and time spent on physical experiments while delivering adequate information for statistically acceptable results. Until now, only a few studies are available in the literature on the application of the RSM in SCW gasification. Yang, et al.[34] applied the RSM to optimize H_2 production from SCW gasification of crude glycerol. Three factors, namely, glycerol concentration, reaction temperature, and KOH concentration were examined. The results showed that the optimum reaction conditions for producing H_2 were at 500 °C with 7 wt % glycerol concentration and 2.39 mol L^{-1} KOH concentration. Samiee-Zafarghandi, et al.[35] reported on the effects of temperature, feed loading, and reaction time on gaseous product's composition of the microalgae after SCW gasification using the RSM. The most critical variable found was the temperature, followed by the reaction time and the microalgal biomass loading. A similar parametric optimization study using the RSM was conducted[28] while studying the SCW gasification of food waste in the literature. The authors found a different order of rank of the significance of different factors, starting with the temperature followed by the residence time and finally the feed concentration. Kang, et al.[36] optimized a noncatalytic gasification of lignin in SCW using the central composite design. Three factors namely temperature, pressure, and biomass ratio were selected. The results showed that the

pressure had the most insignificant influence on the gas yield and that the optimal temperature, water to biomass ratio, and pressure were 651 °C, 3.9%, and 25 MPa, respectively. Lu, et al.[37] explored the effect of four factors (temperature, residence time, pressures, and feedstock concentration) in the SCW gasification of corncobs using an orthogonal experimental design. The effectiveness of these factors was ranked in the order of temperature > pressure > feed concentration > residence time. The disagreement in the order of severity among different factors in the reported literature could be attributed to the level of operating conditions studied, types of biomass used, and the type and configuration of the reactor used. Therefore, it is essential to examine further the optimization of these parameters with a focus on the specific biomass and reactor type. Currently, to the best of our knowledge, there is not a single study that exists on the parametric optimization of sub- and SCW gasification of RH using the RSM.

Thus, in the current study, parametric optimization of sub- and SCW gasification of RH is examined and reported. The operating parameters studied are temperature, residence time, and feed concentration on the GE and gas volume, char, tar, and gravimetric tar yield. These operating parameters predominantly affected the SCW gasification of biomass. Also, for the first time, this study employs a RSM for SCW gasification based on a computer-aided design using the I-optimality criterion. Unlike other classic RSM methods (Box-Behnken and Central-Composite), optimal designs are efficient and reliable for analyzing the optimization problem, and it can fit any model (first and second, quadratic, or cubic orders).[38,39] Furthermore, the I-optimality design affords a reduced number of experimental runs than classic RSM types and offers a constrained design space.

Table 1. Response Transformation and Model Fitting Summary

response	response range	ratio[a]	transformation	fit summary
GE	49.0−64.5	1.3	none	quadratic
tar yield	3.1−18.5	5.9	none	quadratic
char yield	25−39.4	1.5	none	quadratic
gravimetric tar content	109.7−1958.8	17.8	log	quadratic
gas volume	88.4−428.6	4.8	none	quadratic

[a]Ratio of maximum to the minimum response (a ratio >10 suggests response transformation).

2. RESULTS AND DISCUSSION

2.1. Model Fit and Statistical Analysis. Table 2 shows the results from the predicted and experimentally measured responses for the 20 runs according to the Design-Expert software formulated experiments. The GE ranged from 48.96 to 64.45% on dry basis feedstock, and the maximum GE was obtained from the 9th run, under the condition of X_1 = 406 °C, X_2 = 120 min, and X_3 = 3.0 wt %. On the other hand, tar and char yield assumed values from 3.11 to 18.54 wt % and 24.96 to 39.42 wt %, respectively. The lowest tar yield was observed from the 14th run under the experimental condition of X_1 = 500 °C, X_2 = 70 min, and X_3 = 7.8 wt %. The gravimetric tar yield and gas

Table 2. Experimental Variables and Products Distribution of Sub- and SCW Gasification of RH Using I-Optimality Design[a]

				response variables									
	variables			GE (%)		tar yield (wt %)		char yield (wt %)		gravimetric tar yield (g/Nm³)		gas volume (mL/g)	
Run. no	X_1 (°C)	X_2 (min)	X_3 (w %)	exp.	pred.	exp.	pred.	exp.	pred.	exp.	pred.	exp.	pred.
1	500	30	10	57.6	57.5	4.0	4.0	38.3	37.9	147.9	143.6	273.5	266.1
2	353	80	6	53.7	53.0	14.5	14.6	31.8	31.9	1645.9	1509.6	88.4	92.3
3	418	120	8	57.6	58.5	4.3	4.7	38.1	37.2	232.5	274.5	186.9	179.3
4	500	120	7	56.5	57.3	4.1	3.3	39.4	39.8	121.5	110.9	334.8	324.0
5	500	120	3	60.8	60.3	5.0	5.8	34.3	34.1	115.7	123.0	428.6	423.8
6	433	32	6	58.0	58.4	5.0	5.9	36.9	36.0	265.3	303.9	188.8	191.1
7	353	80	6	52.2	53.0	15.4	14.6	32.3	31.9	1722.5	1509.6	89.5	92.3
8	433	32	6	59.0	58.4	5.8	5.9	35.2	36.0	311.0	303.9	186.5	191.1
9	406	120	3	64.5	63.4	7.7	8.3	27.8	28.5	375.5	380.9	206.1	218.4
10	418	57	3	61.9	63.4	9.7	8.7	28.4	28.0	410.8	384.8	235.0	221.4
11	350	30	3	56.5	56.6	18.5	18.9	25.0	24.9	1958.8	2093.9	94.7	97.5
12	452	91	5	61.4	60.9	5.3	4.3	33.2	34.9	201.6	191.4	264.3	258.1
13	433	80	10	59.3	60.0	4.6	4.6	36.1	35.8	255.1	235.2	179.4	181.3
14	500	70	8	57.7	57.4	3.1	3.6	39.2	38.5	109.7	130.9	283.8	302.6
15	433	32	6	58.6	58.4	5.8	5.9	35.6	36.0	313.4	303.9	186.5	191.1
16	500	63	3	59.8	60.1	6.7	6.2	33.5	32.9	165.7	150.4	402.1	407.1
17	433	80	10	61.0	60.0	4.5	4.6	34.5	35.8	250.1	235.2	179.4	181.3
18	350	120	10	50.5	50.6	13.5	13.4	36.0	35.4	1297.0	1291.3	104.2	114.0
19	353	80	6	53.3	53.0	14.2	14.6	32.5	31.9	1347.1	1509.6	105.1	92.3
20	350	30	10	49.0	49.0	16.6	16.4	34.5	35.1	1741.4	1776.9	95.2	87.5

[a]Where: X_1 is the temperature, X_2 is the residence time, X_3 is the feed concentration, exp. is the experimental value, and pred. is the predicted value.

volume ranged from 106.67 to 1958.78 g/Nm³ and 88.37 to 428 mL/g biomass, respectively. The highest gas volume was obtained from the 5th run, under the experimental condition of X_1 = 500 °C, X_2 = 120 min, and X_3 = 3.0 wt %.

The obtained results were fitted to a second-order polynomial model, and the Design-Expert software suggested quadratic models for both responses and log-transformation for gravimetric tar data, as shown in Table 1. The final empirical models in terms of the coded variable (eqs 1−5) were derived after the reduction of trivial terms ($p > 0.1$) through the p-values backward model selection algorithm in the Design-Expert software.

$$GE(\%) = 59.46 + 2.65X_1 + 0.7985X_2 - 2.21X_3 + 1.59X_1X_2 - 4.72X_1^2 - 0.8557X_2^2 + 2.36X_3^2 \tag{1}$$

$$tar\ yield(wt\ \%) = 5.44 - 5.61X_1 - 0.9110X_2 - 1.23X_3 + 0.5744X_1X_2 + 4.10X_1^2 + 0.9902X_3^2 \tag{2}$$

$$char\ yield(wt\ \%) = 35.25 + 2.93X_1 + 0.1607X_2 + 3.58X_3 - 1.53X_1X_3 + 1.12X_2^2 - 3.30X_3^2 \tag{3}$$

$$\log_{10}(gravimetric\ tar\ yield)(g/Nm^3) = 2.47 - 0.5463X_1 - 0.0693X_2 - 0.0356X_3 + 0.2046X_1^2 \tag{4}$$

$$gas\ volume(mL/g\ biomass) = 187.65 + 119.58X_1 + 13.24X_2 - 35.32X_3 - 30.30X_1X_3 + 19.21X_1^2 + 18.47X_3^2 \tag{5}$$

Equation 1−5 can be used to predict the GE, tar, char, gravimetric tar, and gas volume, respectively. Generally, the negative sign signifies the antagonistic effect of the factors, and the positive sign indicates the synergistic effects of the factors. Examining the coefficients and the power of the polynomial model factors, it is clear that the temperature has the most substantial influence on SCW gasification, which is followed by the feed concentration and finally the residence time. In the range of experimental parameters, the results of the experiments show that the order of severity of factors on the GE, tar yield, char yield, and gas volume follows a similar trend: temperature > feedstock concentration > residence time, which is in good agreement with the rank reported in the literature.[37] On the other hand, the trend of factors for the gravimetric tar content follows a different order, that is, temperature > residence time > feedstock concentration. Chen, et al.[28] found a similar trend while experimenting on the gasification characteristics of food waste using SCW. The order of effect may be influenced by the range of operating conditions, reaction configurations, and the type of biomass studied.[28]

To ensure that the derived polynomial model fits well with the experimental data, a test for the significance of the regression model and its coefficient, lack-of-fit, and pure-error is performed. The significant factors are ranked based on the probability value (p-value) with a 95% confidence level. The results of the analysis of variance (ANOVA) for the responses generated by eqs 1−5 are shown in Table 3. A smaller p-value ($p < 0.05$) indicates that both models are significant. Non-significant lack-of-fit ($p > 0.05$) for both derived models implies that the lack-of-fit is not

Table 3. ANOVA for the Response Surface Reduced Quadratic Model

	GE (%)			tar yield (wt %)			char yield (wt %)			gravimetric tar yield (g/Nm³)			gas volume (mL/g)		
	SS	F	p	SS	F	p	SS	F	p	SS	F	p	SS	F	p
model	293.86	56.83	<0.0001	473.29	171.62	<0.0001	264.49	54.44	<0.0001	3.66	450.61	<0.0001	193494.69	296.71	<0.0001
X_1	76.14	103.08	<0.0001	341.79	743.63	<0.0001	93.02	114.88	<0.0001	3.25	1601.31	<0.0001	154830.46	1424.55	<0.0001
X_2	6.46	8.74	0.0120	9.14	19.89	0.0006	0.26	0.32	0.5793	0.05	26.08	0.0001	1779.96	16.38	0.0014
X_3	50.26	68.05	<0.0001	14.21	30.92	<0.0001	132.38	163.49	<0.0001	0.01	6.47	0.0225	12879.64	118.50	<0.0001
X_1X_2				1.81	3.93	0.0690									
X_1X_3	14.00	18.95	0.0009	71.17	154.85	<0.0001	13.02	16.07	0.0015	0.19	92.10	<0.0001	5078.40	46.72	<0.0001
X_1^2	96.99	131.31	<0.0001										1604.43	14.76	0.0020
X_2^2	3.09	4.18	0.064	4.18	9.09	0.0100	5.30	6.55	0.0238						
X_3^2	22.30	30.19	0.0001				44.34	54.76	<0.0001				1401.04	12.89	0.0033
residual	8.86			5.98			10.53			0.03			1412.94		
lack of fit	5.76	1.33	0.3903	4.71	2.33	0.1837	7.19	1.35	0.3874	0.02	1.05	0.5109	1233.31	4.29	0.0627
pure error	3.10			1.27			3.34			0.01			179.62		
cor total	302.73			479.26			275.02			3.69			194907.63		

substantial relative to the pure error, and the models can accurately predict the variations.

The quality of the fitted polynomial model can be determined by R-squared, which represents the proportion of the variability of the data accounted for the statistical model. It is more appropriate also to use Adj-$R2$, which penalizes the statistic R^2 if unnecessary terms are added in the model.[40] The R^2, adjusted R^2, and predicted R^2-value for all responses are close to 1 (>0.9), indicating the accuracy of the predicted polynomial model (Table 4). The predicted R^2 is in reasonable agreement with

Table 4. Model Fit Statistics for the Gasification Yield[a]

	GE (%)	tar yield (wt %)	char yield (wt %)	gravimetric tar yield (g/Nm³)	gas volume (mL/g)
R^2	0.9707	0.9875	0.9617	0.9917	0.9928
adj R^2	0.9536	0.9818	0.9441	0.9895	0.9894
pred R^2	0.9248	0.9714	0.9172	0.9862	0.9814
adeq. precision	26.543	38.675	27.981	56.649	54.525
std. dev.	0.859	0.678	0.900	0.045	10.430
mean	57.45	8.42	34.13	2.59	205.64
C.V. %	1.50	8.05	2.64	1.74	5.07
press	22.76	13.72	22.77	0.05	3633.15

[a]Where CV is the coefficient of variance.

adjusted R^2 for both responses (the difference is less than 0.2) which demonstrate a high correlation between the experimental and the predicted values. Moreover, it implies that the proposed regression models provide an acceptable explanation of the interaction between independent variables and responses.

Adequate precision measures the signal to noise ratio, and the ratio greater than 4 is desirable. In this study, the ratio between 26.54 and 56.65 is obtained, indicating an adequate signal, and it also suggests that the models have a robust signal to be used for optimization. The coefficient of variation (CV) indicates the degree of precision with which the experiments are compared.[41] In this case, a low CV for both regression models (<8.05%) indicates that model reproducibility is satisfactory (Table 4).

To ascertain the validity of the predicted models, the normal probability plots of the residual and experimental versus predicted values are used. The residuals are the difference between the actual and the predicted values. The plots for the normal probability and the externally studentized residuals and the predicted versus actual values for both responses are presented in Figures 1 and 2. The normal probability plots of the residuals and the deleted residuals versus the predicted values for the original gravimetric tar yield data show a clear systematic trend with the S-like shape and a possible funnel-like shape, respectively, which suggests the use of log transformation of the data. Figure 1a—e reveals that the residuals generally distributed along the line of best fit, implying that errors are distributed normally with no abnormality in the models. An observation of Figure 2a—e suggests that the predicted values are in good agreement with the experimental ones, within the design space.

2.2. Interpretation of the Derived Models. Three-dimensional (3D) response surface plot provides the best way to visualize the interactions of the independent and dependent variables and facilitates the optimal condition for response yield. A contour and 3D plots depicting the interaction among the temperature, residence time, and feed concentration on responses provide essential information on the sub- and SCW gasification behavior of RH. A steep or curvature slope in the
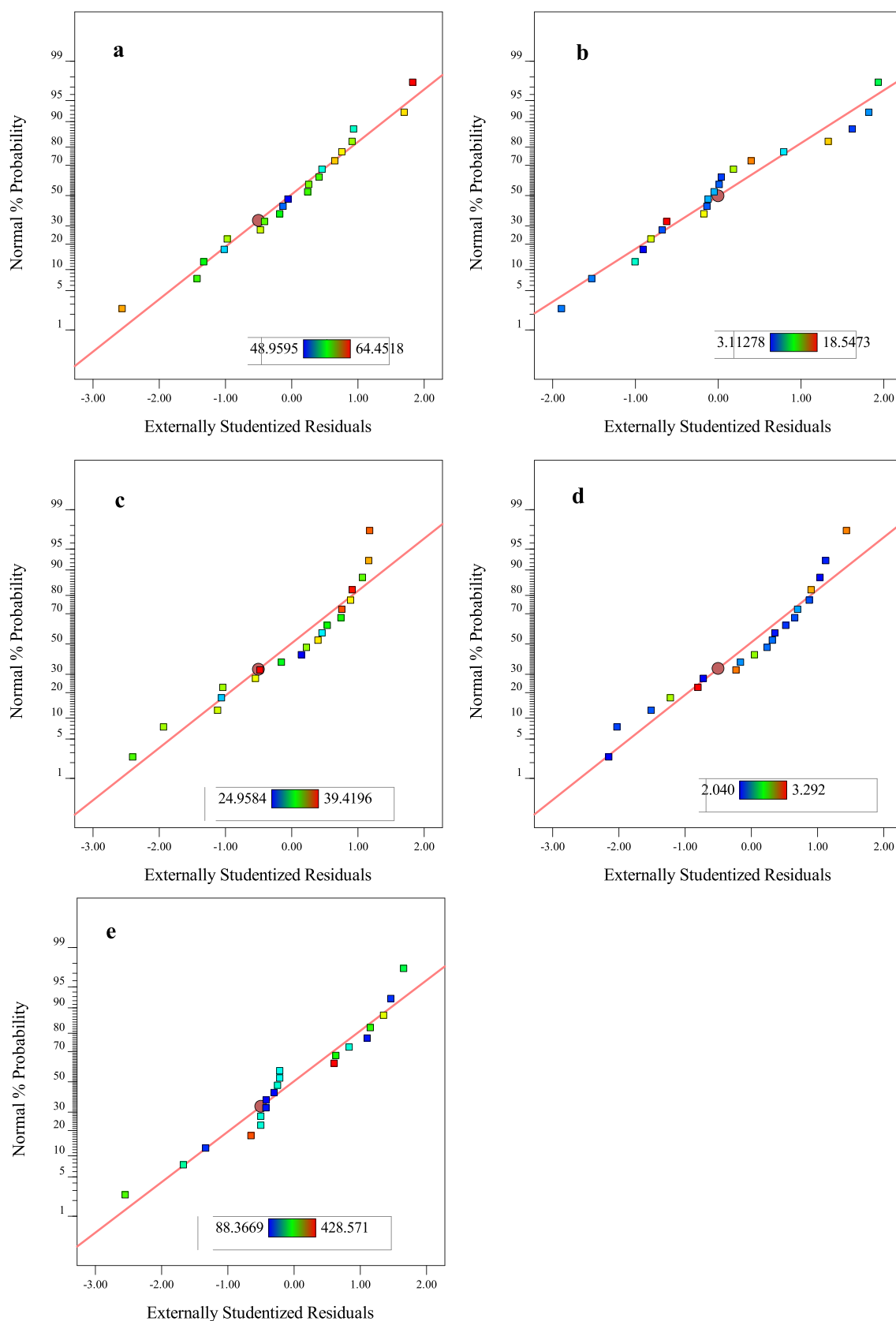
Figure 1. Studentized residuals and normal percentage probability plot for (a) GE, % (b) tar yield, wt %, (c) char yield, wt %, (d) gravimetric tar yield (log-transformed) g/Nm^3, and (e) gas volume, mL/g biomass.

response surface plots accentuates the level of the sensitiveness of the response to a particular factor. A relatively flat surface signifies that any change in the variables is less influential to the variation of response.[42]
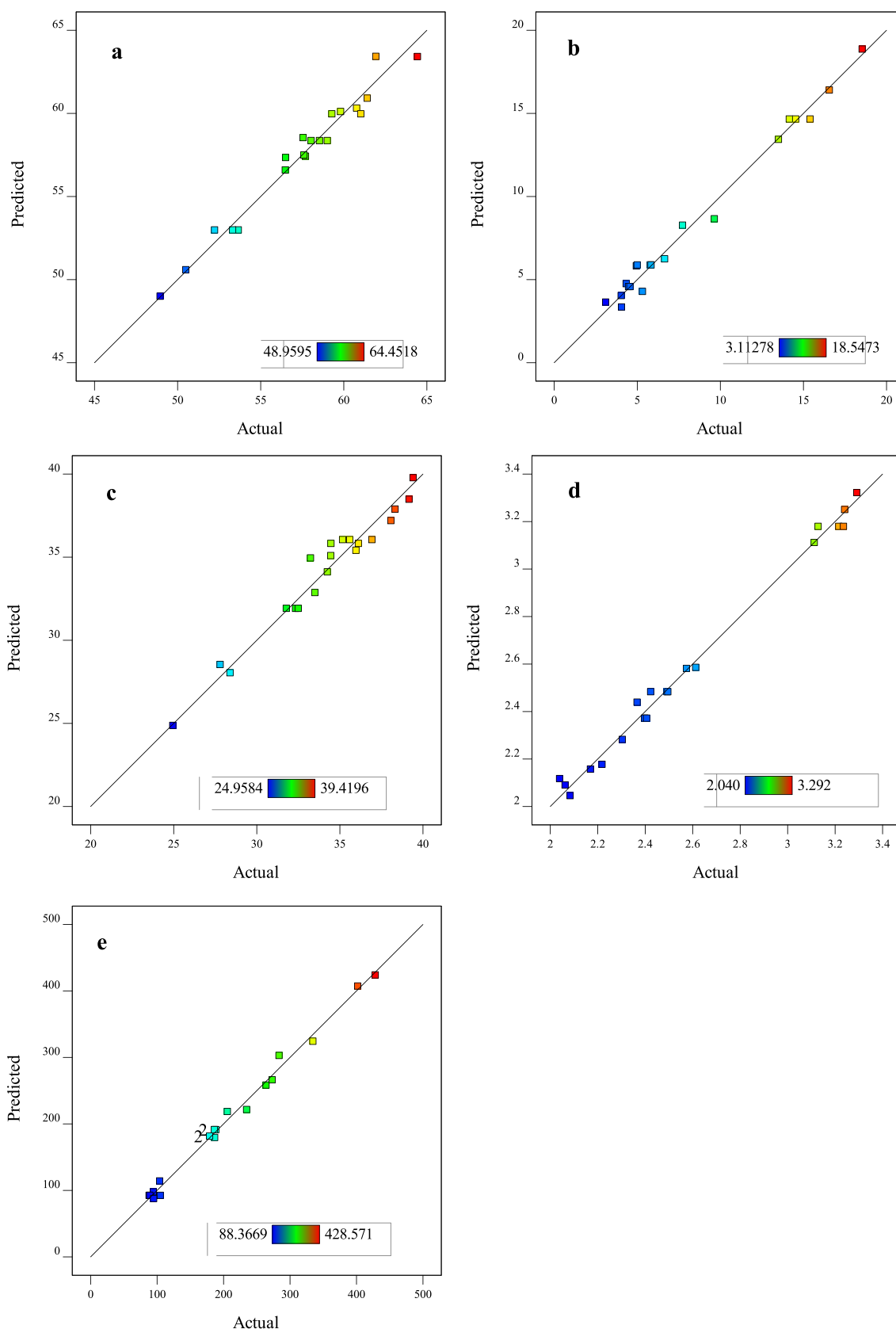
Figure 2. Comparisons of predicted and experimental values of SCW gasification for (a) GE, wt % (b) tar yield, wt % (c) char yield, wt % (d) gravimetric tar yield (log-transformed), g/Nm^3 and (e) gas volume, mL/g-biomass.

2.2.1. Influence of SCW Gasification Parameters on GE. GE is defined as the percentage of the total mass of gas product per total mass of the feed [GE = (the total mass of gas (g)/the mass of dry feedstock (g)) × 100%].[28] The total mass of the gas
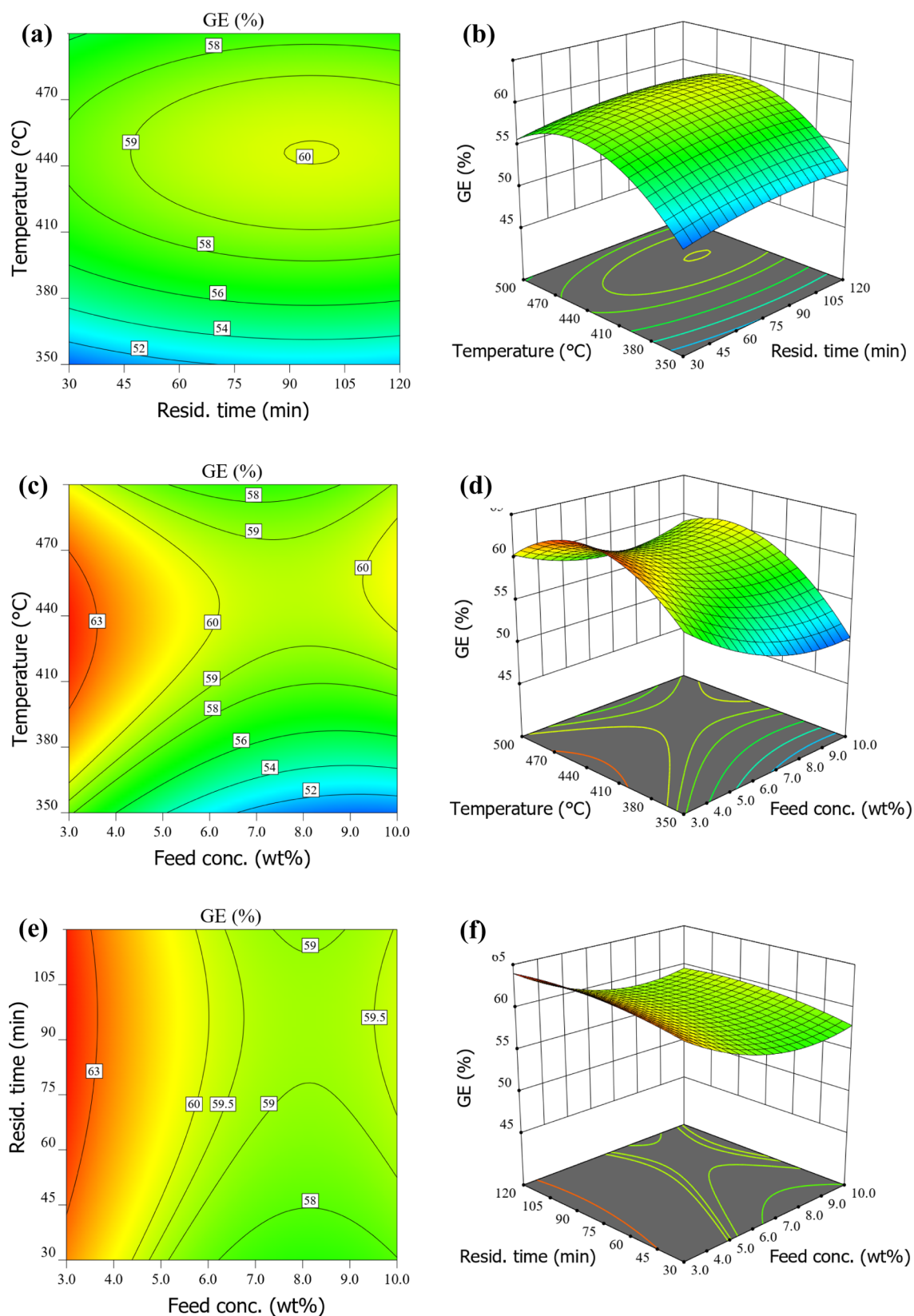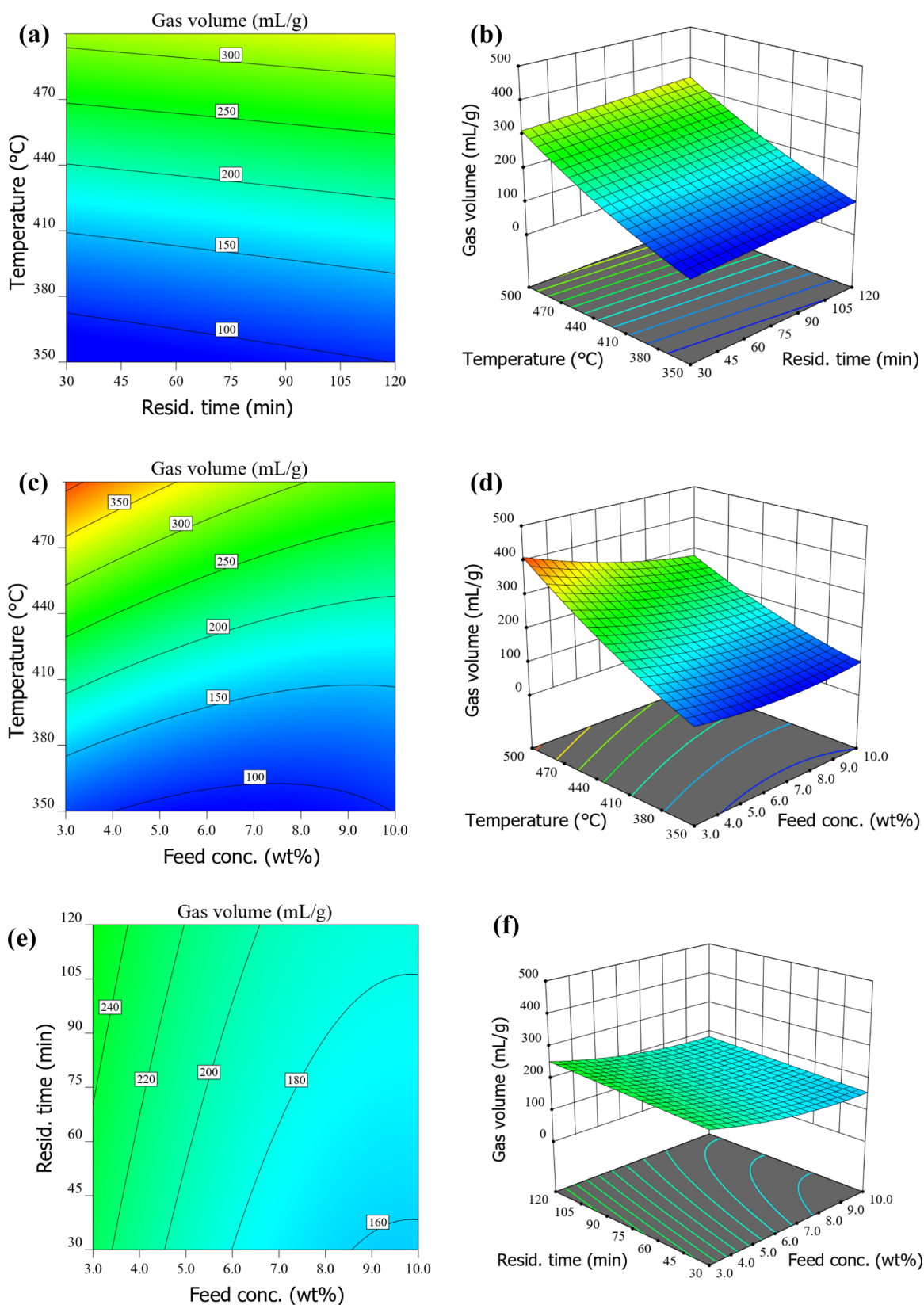
Figure 3. Contour and 3D response surface plots representing different interactive effects of parameters on GE. (a,b) Temperature, residence time, and feed concentration 6.5 wt %, (c,d) temperature, feed concentration, and residence time 66 min, and (e,f) residence time, feed concentration, and temperature 425 °C.

product is obtained by differences (total mass of gas = mass of RH feed − total mass of tar − total mass of char). Figure 3 shows the contour and 3D surface plots for different interaction factors

on GE. Figure 3a,b shows that GE increases with an increase in temperature and residence time at a constant feed concentration of 6.5 wt %. The maximum GE of 60% was attained at a

Figure 4. Contour and 3D response surface plots representing different interactive effects of parameters on gas volume. (a,b) Temperature and residence time, feed concentration 6.5 wt %, (c,d) temperature and feed concentration, residence time 66 min, and (e,f) residence and feed concentration, temperature 425 °C.

residence time of 95 min and a temperature of 446 °C, any further increase of these two factors resulted in a steady reduction of GE. The decrease of GE at higher temperature and

residence time may be attributed to coke or carbon formation as a byproduct of reforming reactions. Coke and carbon formation reactions are discussed in detail in Section 2.2.4.

GE increases sharply with the rise in temperature from 350 to 446 °C due to rapid devolatilization of feedstock but shows a more gradual increase with an increase in residence time due to a slow char gasification reaction.[1] Temperature is determined to be the most crucial parameter in the SCW gasification of biomass; higher temperature maximizes GE and increases the overall gas volume. As temperature increases beyond the critical point, water density decreases, thus resulting in a lower ionic product which favors the shift of ionic mechanism to free radical mechanism. The latter enhances biomass decomposition and favors the reaction forming gaseous product.[2] Promdej and Matsumura[43] investigated the sub- and SCW gasification of the glucose model compound at a temperature range of 300−460 °C and a feed concentration of 1.5 wt %. The study revealed that subcritical water gasification reaction was dominated by ionic mechanisms, indicating low GE due to the insignificant amount of energy for endothermic reaction of breakdown of complex biomass molecules. The observed decrease in GE in our study at a temperature beyond 446 °C could be attributed to coke and carbon formation. This finding is consistent with other existing literature.[44,45] The interaction between biomass concentration and other independent variables (temperature and residence time) Figure 3c,e shows a similar trend whereby the maximum GE of approximately 64.15% was observed at the lowest biomass concentration of 3.0 wt %.

Notably, GE under the condition of biomass concentration 6.2 and 9.3 wt % at a constant temperature of 450 °C and residence time 75 min were similar, being near 60%. Also, similar GE of 58% was observed under the following condition: 407 and 492 °C and a constant biomass concentration of 7.4% and a residence time of 75 min Figure 3c,d. This trend may be influenced by the change of the two competing SCW reaction mechanisms, which are mass transfer and pyrolysis of the feedstock.[28] When the biomass concentration is 3 wt %, the mass transfer between biomass particles and water could be the dominating step in determining the overall reaction rate. When the feed concentration is increased, the mass transfer rate is suppressed, leading to a reduction of the GE. The threshold at which the mass transfer rate starts to change is when the feed concentration exceeds 8 wt %. When the temperature reaches 450 °C and the feed concentration increases from 5.5 to 10 wt %, the transition between the mass transfer mechanism and the pyrolysis of the feedstock occurs; the latter becomes the rate-determining step at a feed concentration of 10 wt %. This leads to a similar GE with different reaction mechanisms for the feed concentration of 5.5 and 10 wt %. These findings are in good agreement with that reported in the literature.[28,46]

In this study, we observed only a slight interaction of residence time with other independent variables in the overall GE. The GE varied slightly from 58.2 to 60% when the residence time increases from 30 to 95 min at 446 °C Figure 3a,b. Moreover, GE is significantly affected by the change in residence time for feed concentration below 5 wt % Figure 3e,f. At a feed concentration of 3 wt %, GE increases from 62.2 to 64.2 wt % when the residence time changes from 30 to 118 min, and then, it begins to decrease, implying that a longer residence will have a small impact on the change of GE. Similarly, as reported in other studies, Wang, et al.[1] noted a sharp increase of GE at residence time below 10 min and only slight variation beyond 15 min while studying the gasification mechanism of biomass in SCW. The impact of residence time was found to be more pronounced at low temperatures (<425 °C) than at higher temperatures.[44] In another study, Susanti, et al.[47] found no significant impact of

residence time on the total GE in SCW gasification of glucose at 740 °C. Reddy, et al.[2] showed that GE increases with residence time, usually in the early stage to a "certain time" and afterward, no significant change resulted. This "certain time" is a function of many operating factors including feedstock properties, feed concentration, reactor type, and reaction temperature.[28] Under the condition of our study (constant feed concentration of 6.5 wt % and temperature 446 °C), the "certain time" was found to be 95 min. This means that a residence time of 95 min was sufficient to some extent to yield higher GE during SCW gasification of RH at the condition of feed concentration 6.5 wt % and 446 °C. In yet another study,[48] reported the "certain time" of 75 min at 480 °C and feed concentration of 5 wt % during SCW gasification of unsorted food waste under the conditions of temperature between 420 and 480 °C, feed concentration of 5−15 wt %, and residence time 30−75 min.

2.2.2. Influence of SCW Gasification Parameters on Gas Yield. Gas volume significantly increases with temperature and is slightly affected by residence time, as shown in Figure 4a,b. The increase in gas volume could be explained by the continuous breakdown of tar to form permanent gases. Figure 4a shows that a gas volume of 75 mL/g is obtained at a temperature of 350 °C, a residence time of 30 min, and a feed concentration of 6.5 wt %, and it rapidly increases to 313 mL/g when the temperature increases to 500 °C. When the residence time increases from 30 to 120 min, the gas volume slightly increases from 313 to 339 mL/g. No significant interaction between the residence time and feed concentration ($P = 0.7287$) is observed, as shown in Figure 4e,f. The results demonstrate a good agreement with the experimental data reported in the literature.[48,49] A close look at Figure 4c,d shows that the maximum gas volume of 410 mL/g could be predicted at 500 °C and a feed concentration of 3.0 wt % while it sharply decreases to 279.3 mL/g when the feed concentration is increased to 10 wt %. At 350 °C and a feed concentration of 3 wt % at gas volume of 111 mL/g is predicted, and it slightly decreases to 100 mL/g when the feed concentration rises to 10 wt %. This implies that both temperature and feed concentration have an influence on the gas volume, particularly significant at the higher reaction temperature. Higher feed concentration has an antagonistic effect on gas yield during the SCW gasification process. The volume of gas decreased abruptly with an increase in feed concentration inhibited presumably by the decomposition reactions of the biomass. Promdej and Matsumura[43] reported a significant decrease in the gas yield by the increase in glucose concentration from 1 to 17 wt %. The increase in feed concentration leads to a low fraction of water, thus impeding the reactions such as water−gas shift (WGS) reaction, backward methanation, and steam reforming (eqs 6−9), all of which utilized water as one of the reactants.[1,28]
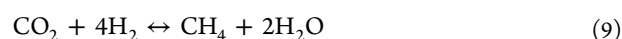
WGS reaction

$$CO + H_2O \leftrightarrow CO_2 + H_2 \tag{6}$$

Steam reforming reaction

$$CH_xO_y + (1 - y)H_2O \rightarrow CO + (1 - y + x/2)H_2 \tag{7}$$

Methanation reaction

$$CO + 3H_2 \leftrightarrow CH_4 + H_2O \tag{8}$$

$$CO_2 + 4H_2 \leftrightarrow CH_4 + 2H_2O \tag{9}$$

To illustrate the reaction behavior inside the reactor, a representative of pressure and temperature for experiment run-4
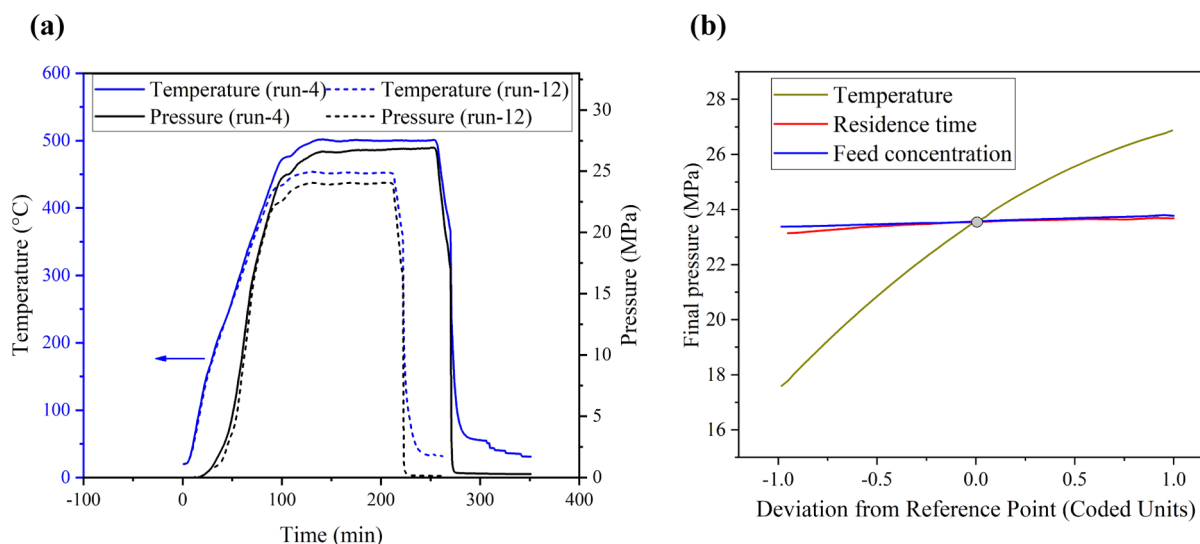
Figure 5. (a) Reaction temperature and pressure versus time for the representative runs no-4 and 12. (b) Perturbation plot showing the effect of variation of temperature, residence time, and feed concentration on final reaction pressure. In all experiments, the reactor was progressively heated from ambient temperature to a destination temperature at an average heating rate of 4 °C/min and maintained for the required residence time.

(500 °C and 120 min residence time) and run-12 (452 °C and 90 min residence time) is presented in Figure 5a. During the residence time, the temperature remained constant while the pressure slowly increased due to a progressive partial gasification of tar to form permanent gas. The final pressure reached in each experiment depends strongly on the feed concentration, reaction temperature, and residence time, as observed by Müller and Vogel.[50] The average final pressure for the conditions studied ranged between 16.8 and 17.8 MPa for subcritical condition and between 22.5 and 27 MPa for the supercritical conditions. Interestingly, we noticed a substantial rise in gas volume with the increase in temperature and residence time, while the efficiency of gasification increased up to a certain temperature and residence time, and then, it began to decrease. This phenomenon can be explained by the change in the composition of gas with the increase in temperature and residence time. The continuous decomposition of CH_4, CO_2, H_2O, and C_nH_{2n} into lighter gases and carbon (eqs 10−14) may increase the gas volume continuously, while observing the drop in GE. In fact, the GE in the current study is determined by the converted gas per total mass of the feed, and the converted gas is obtained by subtracting mass of tar and char from the total feed. Wang, et al.[51] reported a decrease in the fraction of CO_2 and CO as the process time increased from 60 to 1200 s; and significantly increased H_2 was also observed during the study of SCW gasification of depolymerization slag. It is also stated that CH_4 is the dominant product at lower gasification temperature (<420 °C), and there is a competitive process between the formation of CH_4 and H_2 when the temperature rises to near 500 °C. H_2 becomes the main product when the temperature is elevated to above 600 °C while CH_4 decreases dramatically.[52] This is apparent when looking at the perturbation curve of the final reaction pressure against the reaction temperature and residence time (Figure 5b. The fact that the pressure continues to rise as the two parameters increase suggests a steady rise in the volume of the gas generated.

2.2.3. Influence of SCW Gasification Parameters on Tar Production. Tar yield or gravimetric tar content is another aspect of the SCW gasification process affected by the operating conditions (temperature, feed concentration, and residence

time). Tar is the dark brown viscous oil obtained after solvent extraction by hexane and acetone. Tar yield, in this context, is defined as grams of tar per grams of RH feed in a dry basis, while gravimetric tar yield is expressed as grams of tar per normalized volume of gas in cubic meters. The weight of tar includes those water-soluble and water-insoluble compounds.

After the filtration of the reaction mixture before hexane extraction, the liquid effluent that remained displays colors which varied from golden yellow to almost clear liquid depending on the operating temperature. At lower temperature and short residence time (350 °C and 30 min), we observed a golden yellow liquid residual which changes to almost a clear liquid at high temperature and long residence time (500 °C and 120 min), implying that a higher temperature leads to more feed conversion. Moreover, the yellowish color of the effluent means it contains water-soluble compounds. This observation is consistent with other studies reported in the literature.[53,54] Yan, et al.[54] studied the SCW gasification effluent from food waste and observed that at the subcritical condition, the liquid residual contained a high concentration of chemical oxygen demand (COD) and total organic carbon (TOC) which exhibited a yellowish tinge. This suggests that when the temperature increases from 350 to 500 °C, the COD and TOC are largely converted to gas or water-insoluble organic products, which makes the liquid residue clear, similar to that reported by.[29] In our study, it is observed that, after hexane extraction of the filtrate, the liquid residual changed from yellowish to brownish or clear color depending on the operating temperature; this implies that most of the water-soluble compounds were extracted by hexane (steps 5, 9, 10, and 11 in Figure 11).

Contour and 3D surface plots for different interactions of factors in tar and gravimetric tar yield are shown in Figures 6 and 7, respectively. Figures 6a,b and 7a,b illustrate the interaction of temperature and residence time on tar yield and gravimetric tar content, respectively. At a constant feed concentration of 6.5 wt %, the highest tar yield of 16.6 wt % is observed at 350 °C and a residence time of 30 min, while the lowest tar yield of 2.98 wt % is achieved at 471 °C and a residence time of 120 min as shown in Figure 6a,b. On the other hand, the highest gravimetric tar
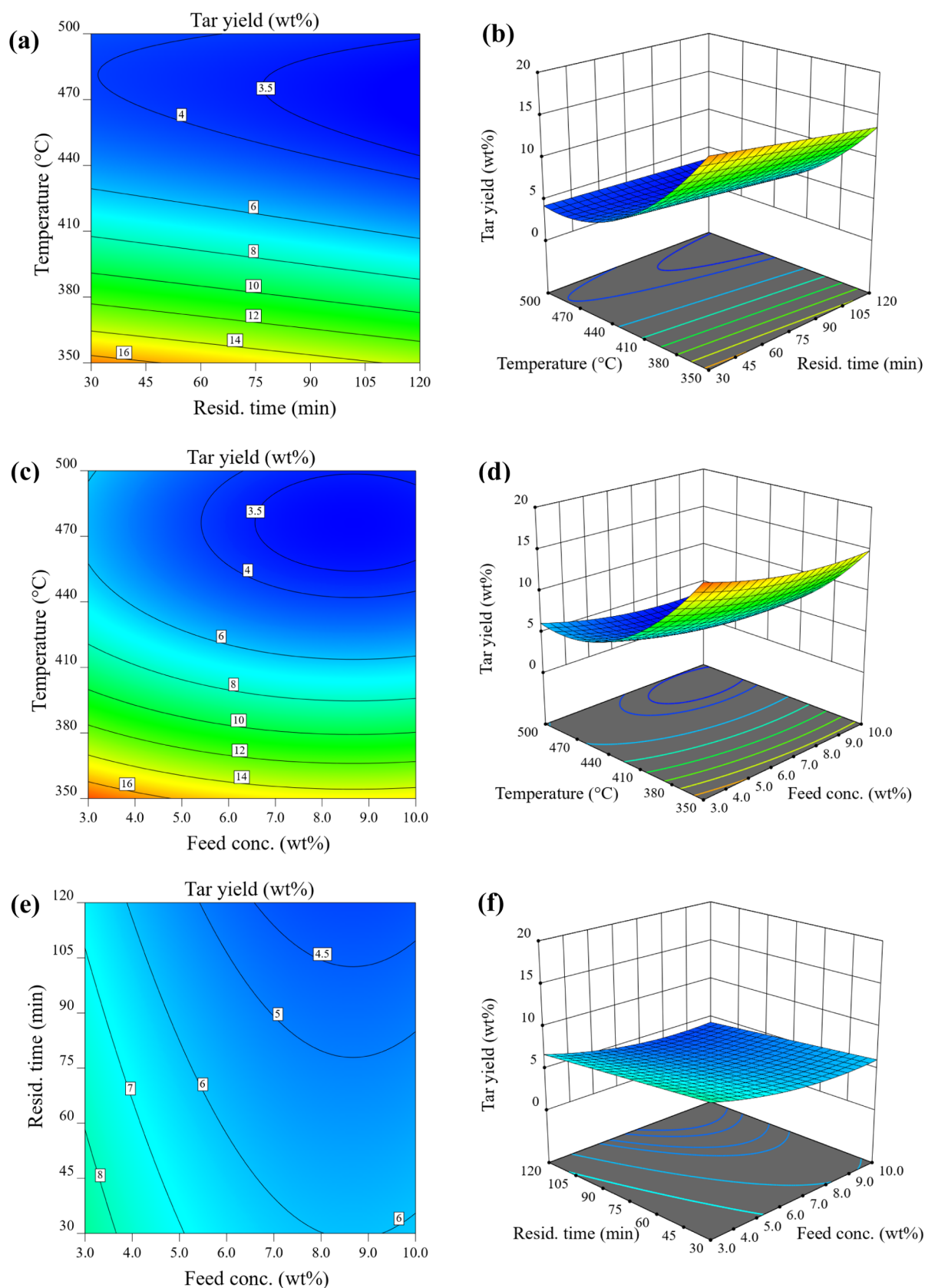
Figure 6. Contour and 3D response surface plots representing different interactive effects of parameters on tar yield (a,b) temperature and residence time, feed concentration 6.5 wt % (c,d) temperature and feed concentration, residence time 66 min (e,f) residence and feed concentration, temperature 425 °C.
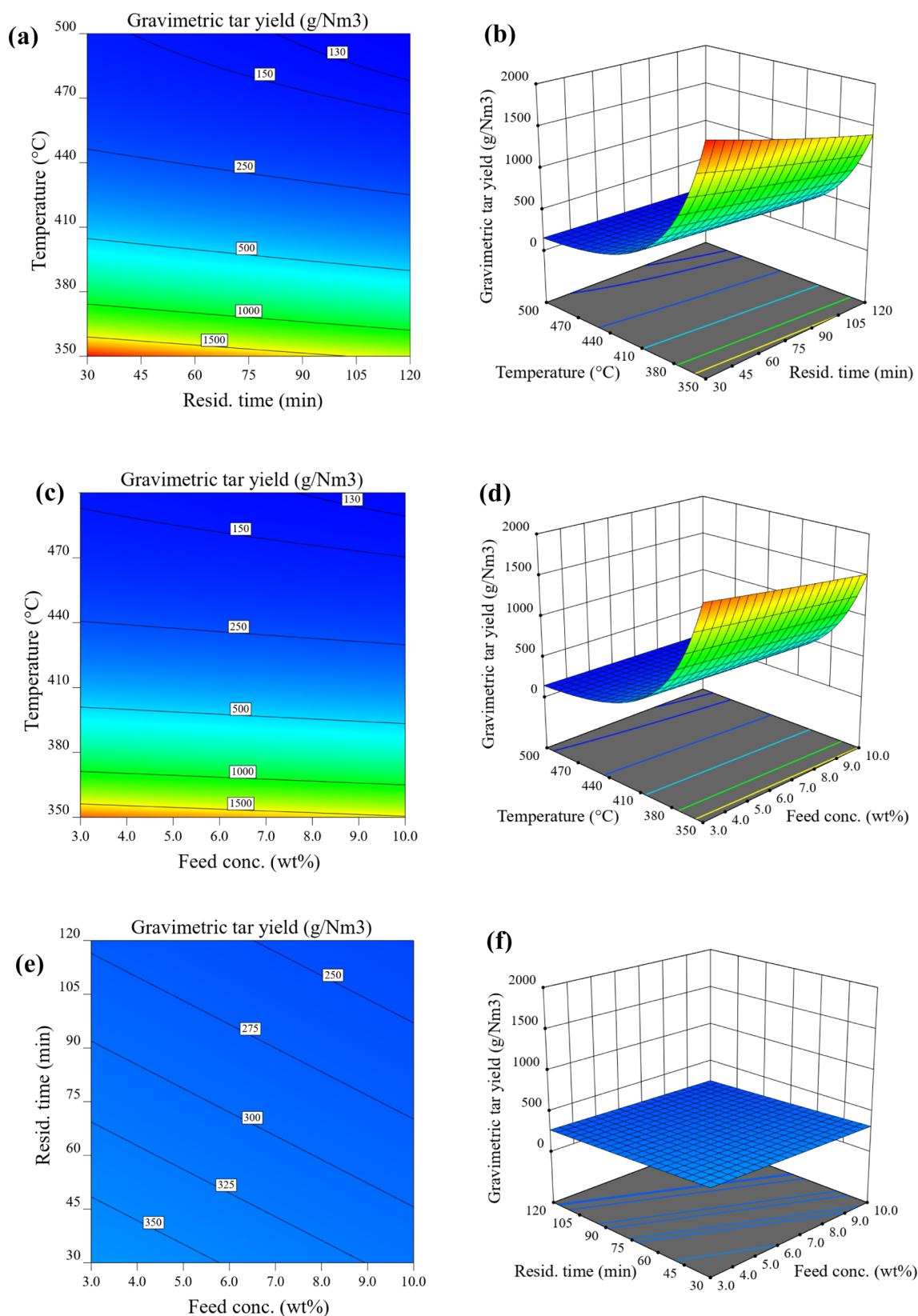
Figure 7. Contour and 3D response surface plots representing different interactive effects of parameters on gravimetric tar yield. (a,b) Temperature and residence time, feed concentration 6.5 wt %, (c,d) temperature and feed concentration, residence time 66 min and (e,f) residence and feed concentration, temperature 425 °C.

content of 1911 g/Nm^3 is seen at 350 °C and a residence time of 30 min, while the lowest value obtained is 114 g/Nm^3, occurring at 500 °C and a residence time of 120 min. The increase in

temperature has the most substantial impact on the overall tar production, which could be explained by the continuous breakdown of tar compounds to form gas or coke. Moreover,
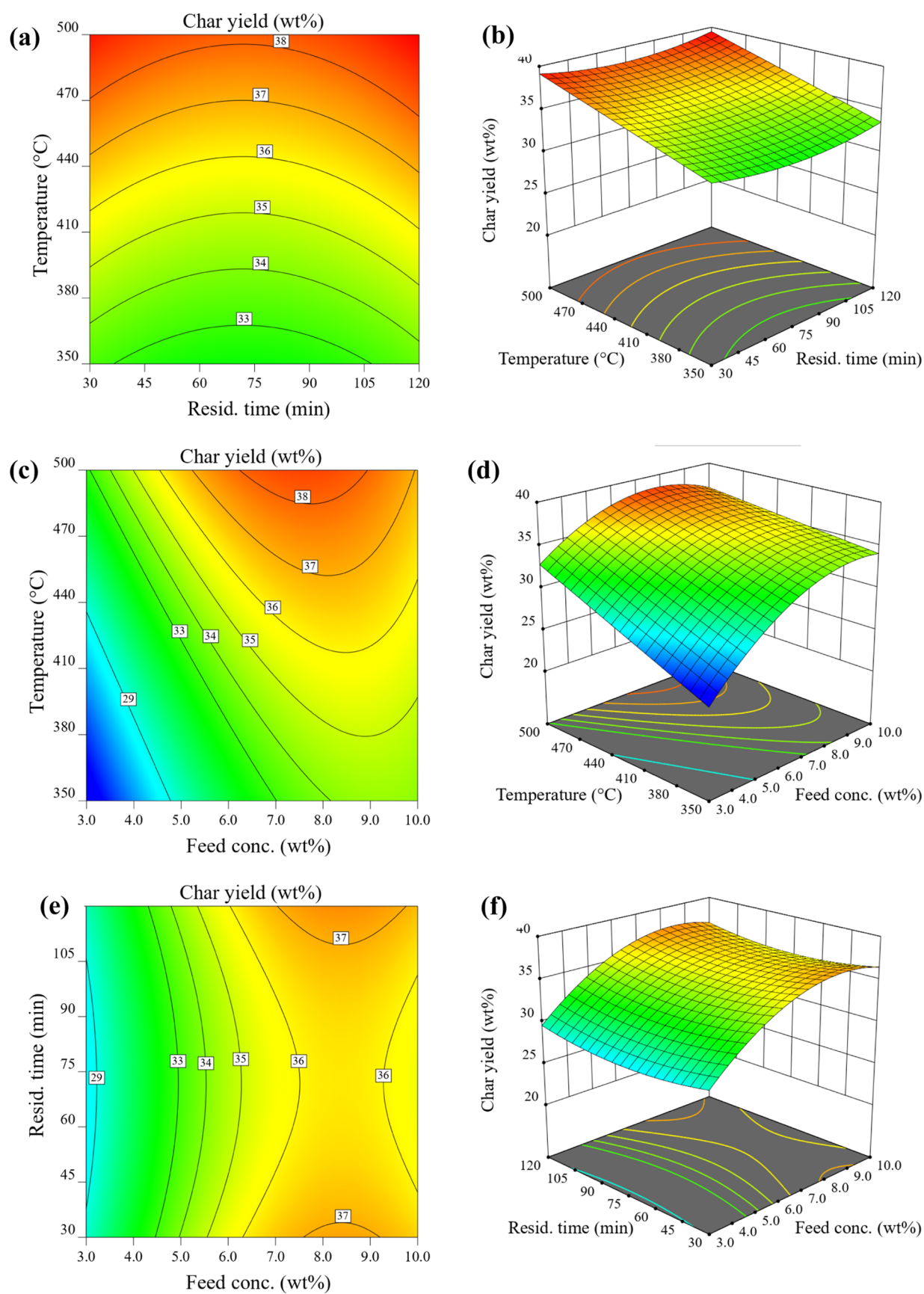
Figure 8. Contour and 3D response surface plots representing different interactive effects of parameters on char yield. (a,b) Temperature and residence time, feed concentration 6.5 wt %, (c,d) temperature and feed concentration, residence time 66 min, and (e,f) residence and feed concentration, temperature 425 °C.
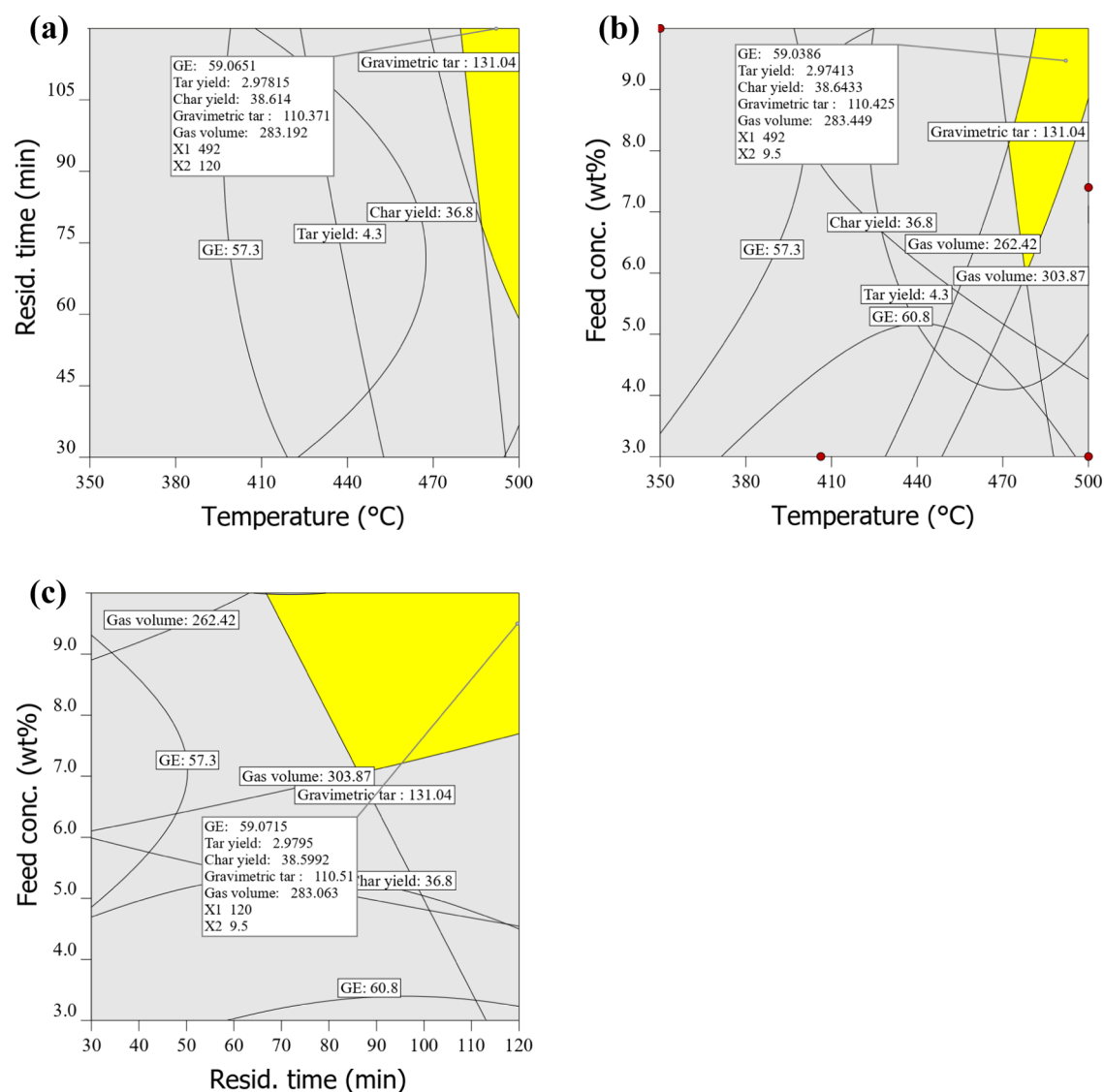
Figure 9. Overlay plot showing the best compromise region for optimal tar yield as a function of (a) temperature and residence time at feed concentration 9.5 wt %, (b) temperature and feed concentration and residence time 120 min and (c) residence time and feed concentration at temperature 492 °C.

a long residence time allows more decomposition of tars to form gas and thus enhances the conversion of feedstock in SCW.

2.2.4. Influence of SCW Gasification Parameters on Char Yield. Char is one of the unwanted products in the SCW gasification of biomass; it, in fact, causes a reduction of the carbon GE. In this paper, char yield is defined as the total weight of any solid leftover after the reaction, which includes ashes, unreacted carbon, and coke formed during the reaction, per weight (gram) of feed. Contour and 3D surface plots for different interaction of factors in char yield are shown in Figure 8. It is seen that the variation of temperature strongly influences the char yield. In particular, Figure 8a,b illustrates that the lowest char yield of 33.1 wt % is obtained at 350 °C and a residence time of 75 min, while the highest char yield of 39.4 wt % is obtained at 500 °C and a residence time of 120 min. This clearly demonstrates that char yield increases significantly with temperature and slightly with residence time. This is probably due to the formation of coke or carbon promoted more at higher reaction temperature due to the cracking mechanism of hydrocarbon. Our findings are in good agreement with data

reported by[55] who studied the gasification of the iso-octane model compound in SCW gasification. Susanti, et al.[55] observed considerably more coke when the gasification was performed at a higher temperature as compared to that at a lower temperature. It is postulated that SCW gasification of biomass takes place in a complicated pathway, one of which is the decomposition of biomass to form intermediate products which are then broken down into gases, char, and liquid via a different mechanism. Furthermore, the intermediates formed underwent decomposition reactions during the release of gases to generate new intermediate molecules.[32] The carbon-containing substances may be formed due to polymerization and condensation of the water-soluble compounds. At the same time, the water-insoluble fraction is pyrolyzed to form a blackened biomass solid which resembles the original biomass. Chuntanapum and Matsumura[56] postulated that the low-molecular-weight acids, aldehydes, and ketones are the intermediate molecules responsible for the gas yield while the ring compounds are responsible for the polymerization reactions yielding char particles. Minowa, et al.[17] examined the cellulose decomposition
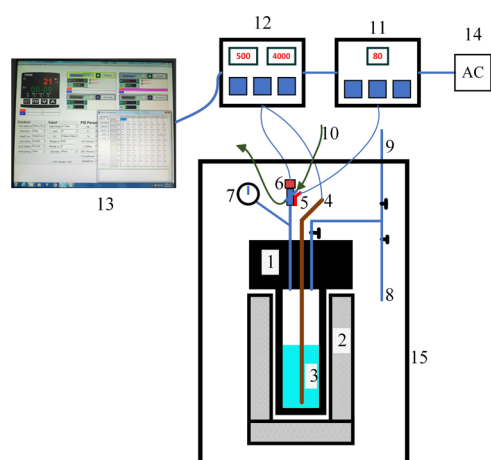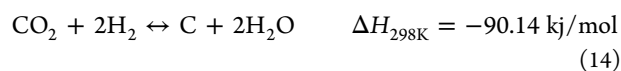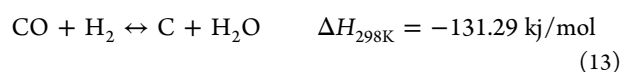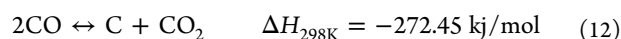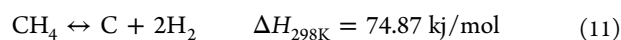
Figure 10. Scheme diagram of the reactor assembly: (1) reactor (2) furnace (3) reaction mixture (4) thermocouple (internal temperature measurement) (5) thermocouple (transducer temperature measurement) (6) transducer (7) analog pressure gauge (8) nitrogen line (9) gas sampling/venting line (10) coolant line (11) master controller (12) reactor controller (slave) (13) communication software (14) power source (15) safety cabin.

in hot compressed water and suggested that cellulose first decomposes to form soluble compounds and oils. With an increase in reaction temperature, the soluble compounds decompose to form permanent gases while the oil decomposes to form char and gas. These results are in good agreement with our findings where low char and high tar yield at lower temperature and a high char and low tar yield at high temperature are exhibited. It is evident that at higher temperature, tars decompose to form gas and char particles. In SCW gasification, a complex chemical reaction takes place, including biomass reforming, pyrolysis, methanation reactions and WGS, which are responsible for gas formation. However,

other reaction such as polymerization of intermediate products to form coke (eq 10), methane cracking (eq 11), Boudouard coking (CO disproportionation) (eq 12), CO hydrogenation (eq 13), and CO_2 hydrogenation (eq 14) can compete with the primary reaction to form coke and carbon.[57,58]

The feed concentration significantly affects the char yield Figure 8c−f. As the feed concentration increases, the total char yield significantly rises. The deficiency of water at high feed concentration may be one of the reasons for the high char yield due to inhibition of gasification reactions. Moreover, high char yield could be influenced by the absence of the catalyst, which plays an important role to inhibit char formation from oil conversion. The use of catalysts is one of the efficient way to improve the gasification degree; it can accelerate gasification reactions that leads to an increase of gas yield and minimize char formation.[59] Gasification reactions in SCW gasification are stated to be more effective when the concentration of feed is less than 10 wt %.[32]

$$C_xH_yO_z \rightarrow coke \tag{10}$$

$$CH_4 \leftrightarrow C + 2H_2 \qquad \Delta H_{298K} = 74.87 \text{ kj/mol} \tag{11}$$

$$2CO \leftrightarrow C + CO_2 \qquad \Delta H_{298K} = -272.45 \text{ kj/mol} \tag{12}$$

$$CO + H_2 \leftrightarrow C + H_2O \qquad \Delta H_{298K} = -131.29 \text{ kj/mol} \tag{13}$$

$$CO_2 + 2H_2 \leftrightarrow C + 2H_2O \qquad \Delta H_{298K} = -90.14 \text{ kj/mol} \tag{14}$$

2.3. Optimisation of the Responses and Validation of the Model. In this study, RSM using the I-optimality criterion was employed to establish the optimum operation parameters for SCW gasification of RH. The numerical optimization was carried out by using the Design-Expert software to analyze the preliminary experimental results. In general, the SCW gas-
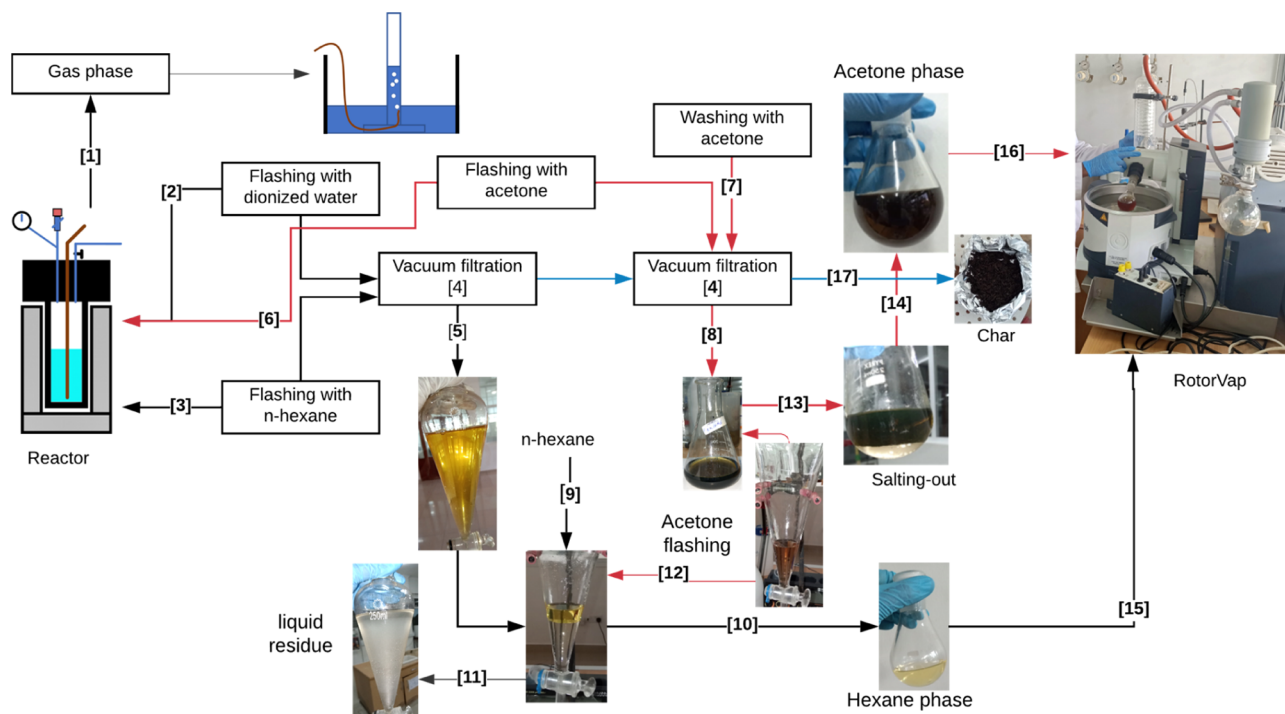

Figure 11. Work-up sequence for the reaction mixture recovery.

ification of lower biomass concentration consumes extra heat energy to raise the temperature of the water, while the high biomass concentration suffers from system plugging.[2] Hence, high feed concentration is used for the reason of attaining high-energy efficiency.[35] High temperature and long reaction time of gasification favor high gas yield; however, these conditions also contribute to higher energy consumption, not to mention increased complexity in vessel design and cost in construction materials.

Therefore, by optimizing the SCW gasification process here, we aim to realize the optimum condition for high GE. In addition to GE, other products including tar yield, char yield, gravimetric tar yield, and gas volume were considered as independent responses in SCW gasification of RH. Table 5

Table 5. Predicted Values of Responses at the Optimized Operating Conditions[a]

| responses | optimum operating condition | | | responses | | |
	temp. (°C)	resid. time (min)	feed conc. (wt %)	goal	pred.	des.
GE (%)	433	96	3	max	64.27	0.989
tar yield (wt %)	492	120	9.5	min	2.98	0.988
char yield (wt %)	355	37	3	min	24.9	1
gravimetric tar (g/Nm^3)	500	106	10	min	109.7	1
gas volume (mL/g biomass)	500	120	3	max	423.8	0.986

[a]Where; tyemp. is the temperature, resid. Time is the residence time, feed conc. is the feed concentration, pred. is the prediction value, des. is the desirability, max is maximize, and min is minimize.

shows the optimum conditions for each independent variable in meeting the required goals for each response. As expected, the selected gasification condition for RH, at a feed concentration of 3 wt %, a maximum temperature of 500 °C, and a duration of 120 min, leads to the highest gas volume of 423.8 mL/g biomass. Moreover, the optimum condition for minimum tar yield of 2.98 wt % could be archived at 492 °C, 120 min and 9.5 wt % RH loading. The desirability value near one shows that the optimization criteria are well satisfied with imposed constraints.

With multiple dependence factors, the optimum condition where all factors simultaneously meet the desirable condition for optimum tar yield could be envisaged graphically by super-imposing the contours of the response in an overlay plot. The overlaying of contour plots (Figure 9) constructed with the combination of three independent factors allows searching visually for a compromised region while satisfying different response requirements. A two-sided confidence interval of 95% was used to obtain high and low prediction intervals. The prediction interval of the response is considered as the acceptable response range within the optimum space. With this interval, we can predict the ranges for individual observations rather than the mean value. The intervals used to construct the overlay plots in Figure 9 were adopted to generate the outcomes as shown in Table 6. The overlay plots show the intervals for predicting the optimum tar yield and other responses over the set range of the independent variables. The yellow shaded region defines the acceptable factor settings while the gray shaded one shows the unacceptable operating condition.

Table 6. Criteria Used for Constructing Overlay Plots

response	95% PI low	predicted value	95% PI high
GE (%)	57.3	59.07	60.83
tar yield (wt %)	1.64	2.98	4.31
char yield (wt %)	36.80	38.62	40.43
gravimetric tar yield (g/Nm^3)	91.97	110.37	131.04
gas volume (mL/g biomass)	262.42	283.15	303.88

The validity of the predicted models was assessed by running three replicates of confirmation experiments at the optimum operating condition for minimization of tar yield. Table 7 shows

Table 7. Predicted and Experimental Values at Optimum Conditions for the Minimization of Tar Yield (492 °C, 120 min, 9.5 wt %)

responses	predicted value	experimental value[a]	RSE (%)
GE (%)	59.07	59.59 ± 0.4	0.8
tar yield (wt %)	2.98	2.95 ± 0.03	1.0
char yield (wt %)	38.62	37.46 ± 0.38	3.0
gravimetric tar (g/Nm^3)	110.37	103.10 ± 1.13	6.5
gas volume (mL/g biomass)	283.15	286.20 ± 2.14	1.0

[a]Is the average of triplicate runs.

the results for the residual standard error (RSE) obtained using eq 15; here, the RSE value of less than 6.5% implies an excellent agreement of experimental values with the model predicted results.[60]

$$RSE(\%) = 100 \times \frac{|(exp.\ value - pred.\ value)|}{pred.\ value} \quad (15)$$

3. CONCLUSIONS

In this paper, the effects of the operating parameters namely reaction temperature (350−500 °C), residence time (30−120 min), and feed concentration (3−10 wt %) on SCW gasification of RH were experimentally studied. The changes in GE, gas volume, tar, char, and gravimetric tar yield were analyzed using the RSM based on the I-optimality design. The conclusions are summarized as follows:

1. By using the RSM involving I-optimality design, quadratic models were obtained for both responses and the predicted values by the models were in excellent agreement with the experimental values. The reaction temperature is the utmost influential factor affecting SCW gasification, followed by feed concentration and, finally, residence time.

2. The GE increased with the rise of temperature and residence time at a constant feed concentration to a "certain time", and after that it started to decrease. The highest GE of 64.2% could be effectively predicted under the condition of 433 °C, 96 min, and a feed concentration 3 wt %, while the minimum tar yield of 2.98 wt % was observed for the condition of 492 °C, 12 min, and a feed concentration of 9.5 wt %.

3. Char yield increased with the rise of reaction temperature and feed concentration, being caused by unwanted char/coke formation as a competing reaction to the main SCW gasification reactions. Therefore, our future study on the utilization of in situ solid catalysts in order to enhance char gasification and accelerate the gasification reactions

Table 8. Physical and Thermochemical Characterization of RH

						physical characterisation	
	thermochemical characterization[a]					particle size distribution	
proximate analysis (wt %)		ultimate analysis (wt %)		heating value (MJ/kg)		sieve no.	pass (%)
moisture content	6.7 ± 1.1	C	33.0 ± 0.67	HHV	13.04 ± 0.08	4	100
volatile matter	58.1 ± 0.23	H	4.5 ± 0.16	LHV	12.42 ± 0.08	2	59.4
ash content	22.4 ± 0.27	N	1.3 ± 0.04			1.5	29.4
fixed carbon[b]	19.5 ± 0.23	O[b]	31.6 ± 0.7			1	11.6
		C/N	26.2 ± 1.3			0.75	5.6
						0.5	3.0
						bulk density (kg/m^3)^a	149.3 ± 1.1

[a]Where means of triplicate determination and. [b]By difference.

in general by suppressing the unwanted reaction pathways leading to char formation is desirable.

4. MATERIALS AND METHODS

4.1. Feedstock Preparations and Characterization. RH was chosen as the feedstock for this study because it is a readily available by-product from the rice processing plant. The sample was collected from a small rice processing plant in Dodoma, Tanzania. The sample was dried overnight in the oven at 105 °C and stored in an airtight plastic bag for further analysis. The results of thermochemical analyses, including ultimate analysis (ASTM D5373-16), moisture content (ASTM E981-82), volatile matter (ASTM D1762-84), ash content (ASTM D1102-84), fixed carbon (by difference) and heating value (ASTM E711-87), and other physical characteristics such as bulk density (ASTM E873-82) and sieving analysis (ASTM C136/C136M-14), are summarized in Table 8.

4.2. Batch Reactor System. The SCW gasification experiments were performed in a batch autoclave made from a type 316 stainless steel (Parr 4650 series, Parr Instrument Company, Moline, IL). The designed working volume, maximum operating temperature, and pressure of the reactor are 500 mL, 600 °C, and 34 MPa, respectively. The reactor system composed of a cylindrical vessel, a type J-thermocouple, electric furnace, reactor controller, analog pressure gauge, a pressure transducer, a pressure relief valve, a needle valve, and a data acquisition system for monitoring and collecting of pressure and temperature data. The electric furnace was controlled to heat the reactor to a specific heating rate and residence time as per experiment requirement. The thermocouple was inserted through a thermowell to detect the internal temperature of the reactor, and the pressure transducer was used to detect the reaction pressure. For this work, we installed a second reactor controller (a master controller) which allow the whole system to operate only when the transducer temperature is below 80 °C, assuring accurate pressure detection by a transducer. Figure 10 shows the scheme diagram of the sub- and SCW gasification system.

4.3. General Experimental Procedure. The dried RH sample (RH) was crushed in a grain milling machine and sieved to obtain a particle size between 0.25 and 0.35 mm. For each experimental run, the RH sample was mixed well with deionized water according to feed concentration requirement (details in Section 4.5) before being loaded into the reactor. Then, the reactor was sealed by using a flexible graphite gasket and carefully tighten by applying 50 Nm torque to each closure bolts. The air inside the reactor was expelled by purging nitrogen gas. The nitrogen pressure of 2 MPa was purged four times to ensure

all the air is evacuated. During the purging process, a pressurized reactor was held for 1 h to observe any decrease in pressure due to leakage. Afterward, a venting line was bubbled in water to ensure no nitrogen left in the reactor.

The reactor was then inserted into the furnace and then programmed using a berrcom temperature controller communication software ver.1.0.0.9 (Parr Instrument Company, Moline, IL) according to temperature and residence time requirement. After reaching the targeted condition, the reactor was rapidly cooled to below 350 °C by blowing cold air externally before lifting and quickly quenched to a cold-water bath to reach ambient temperature. After cooling down, the gas fraction was emptied through a needle valve connecting tygon tubing and measured volumetrically using a water gasometer. The total volume of gas was measured with ±10% accuracy. Then, the reactor was demounted using a wrench, and the remaining reaction mixture was recovered according to a work-up procedure explained in Section 4.4. In summary, this study covers a subcritical water condition (<374 °C and <22 MPa) and a SCW condition (>374 °C and >22 MPa), a residence time from 30 to 120 min, and a feed concentration from 3 to 10 wt %.

4.4. Work-Up Procedures for Reactor Content Recovery. Based on the work-out procedures described by Sato, et al.,[19] Guan, et al.,[16] and Sun, et al.,[30] a new sequential procedure for reaction mixture recovery and tar extraction was developed in this study. In the mentioned studies, the author emptied the reactor and washed the reaction mixture with distilled water and filtration, resulting in an aqueous phase containing water-soluble tars and solid residuals. This method is sufficient for experiments with high biomass conversion and slight or no dissolved tars. Preliminary experiments showed that after washing with deionized water, a significant amount of tars dissolved in the solid char and other substances smeared on the inside walls of the reactor, requiring extraction by dissolving them in an organic solvent. In our developed protocols for tar recovery, distilled water, acetone, and n-hexane mixture were chosen because they are all nontoxic. Hexane dissolves nonpolar compounds, and it has very low solubility in water (0.0095 g L^{-1}) while acetone dissolves the polar tars. Moreover, both organic solvents have low boiling points (acetone, 56 °C and n-hexane, 69 °C); hence, they can be recovered without significant evaporation of the sample.

A sequential procedure for tar and char recovery is shown in Figure 11 (numbers in brackets shows the chronological order of the recovery process). First, the contents in the reactor are transferred into a clean beaker, and then, the experiment setup is flashed three times by deionized water and then by n-hexane, which is then transferred into the same beaker. The setup is

further flashed by acetone which is transferred into a different beaker. The obtained hexane phase is filtrated by the vacuum filtration unit using a Whatman qualitative filter paper no. 1, and the filtrate is transferred to a separating funnel. Tarry compounds dissolved in the filtrate are extracted by the liquid−liquid extraction technique using *n*-hexane. During hexane extraction, polar tars emulsified into the filtrate phase and sticky to the walls of the separating funnel. The separating funnel is then washed by acetone to dissolve all tars, and the obtained solution is transferred to a conical flask. The acetone phase extracted from the experimental setup is filtrated through the same filter paper used for the hexane filtration, and more acetone is added to extract all tars dissolved in the filter cake. The obtained acetone phase is poured into the conical flask containing the rinses from the funnel. After this step, a transparent aqueous layer is resulted, in addition to a tar-free char, a yellowish hexane phase and a dark brown acetone phase. The hexane phase is further dried by using anhydrous sodium sulfate. The acetone phase contains a high quantity of dissolved water and is recovered through a salting-out technique using anhydrous calcium chloride. The water-dry hexane and acetone phases are recovered in a rotary evaporator (Heidolph Instruments GmbH & Co. KG, Germany) at temperature 60 °C, vacuum 870 mbar, and 113 rpm for 10 min each phase. The char fraction is dried in the oven at 105 °C for 4 h and cooled down in a desiccator. The tar and char are gravimetrically weighed using a high precision analytical balance (Ohaus Explorer; accuracy ±0.1 mg); composition characterization of gas and tar is beyond the scope of this paper.

4.5. Experimental Design and Statistical Analysis. RSM is an empirical modeling method for establishing the interaction between numerous operating and response variables. It provides a systematic experimentation strategy for building and optimizing an empirical model. In essence, the RSM is a combination of mathematical and statistical approaches that are suitable for modeling and analyzing problems in which the output is affected by input variables and their interactions.[40] In the current study, a RSM based on the I-optimality criterion was used for the optimization of three independent and five response variables. Independent variables studied are reaction temperature (350−500 °C), residence time (30−120 min), and feed concentration (3−10 wt %) while the observed responses were GE (%), tar and char yield (wt %), gravimetric tar content (g/Nm^3), and gas volume (mL/g biomass). The I-optimality RSM comprises of ten model points, five replicate points, and five lack-of-fit points, implying that 20 experimental runs were required as shown in Table 2. The RSM involves five steps: first, the development of statistically designed experiments, which is followed by generating an empirical model, statistical analysis of the model, and numerical optimization by using desirability function and finally model confirmation.

The experimental run was randomized in order to diminish the error and effect of uncontrolled factors.[61] The observed responses were used to generate an empirical model, which conform to the experimental variables using a quadratic eq 16.

$$Y = \beta_o + \sum_{i=1}^{n} \beta_i X_i + \sum_{i=1}^{n} \beta_{ii} X_i^2 + \sum_{i=1}^{n} \sum_{j=i+1}^{n} \beta_{ij} X_i X_j + \varepsilon$$

(16)

where Y is the predicted response, β_o is the intercept, β_i is the linear coefficient of terms, β_{ii} is the square effect terms, β_{ij} is the interactive coefficient of terms, ε is the fitting error, and X_i and X_j are the coded value of independent variables.

Experimental results from the 20 runs were used for the determination of the regression coefficient of the second-order polynomial models using Design-Expert Version 12.0.3 software (Stat-Ease, Inc., Minneapolis, USA). The coefficient of R-squared established the accuracy of the fitted model, and the significant model terms were assessed by the probability value (P-value) at a 95% confidence level. The contour and the 3D surface plots were generated for the interaction of two independent variables while holding the third variable at the central value. The geometry of the surface plots generated provides useful information about the behavior of the system on the variation of the processing parameter within the design space.

The SCW gasification conditions were numerically optimized using a desirability function of Design-Expert software for the minimization of tar yield. By using the models created during analysis, the best-operating conditions that meet the defined goals were searched within the design space. Finally, one solution among the recommended solutions was selected for the model validation, whereby three replicates of experimental runs were conducted, and results were compared with the predicted values.

■ AUTHOR INFORMATION

Corresponding Authors

Ramadhani Bakari − *Department of Materials, and Energy Sciences and Engineering and African Center of Excellence for Water Infrastructure and Sustainable Energy Futures (WISE-Futures), The Nelson Mandela African Institution of Science and Technology, Arusha 23000, Tanzania; Department of Petroleum and Energy Engineering, The University of Dodoma, Dodoma 41000, Tanzania;* orcid.org/0000-0002-8981-3563; Phone: +255762 830 631; Email: bakarir@nm-aist.ac.tz

Yusufu A. C. Jande − *Department of Materials, and Energy Sciences and Engineering and African Center of Excellence for Water Infrastructure and Sustainable Energy Futures (WISE-Futures), The Nelson Mandela African Institution of Science and Technology, Arusha 23000, Tanzania;* orcid.org/0000-0002-0106-2081; Phone: +255655825866; Email: yusufu.jande@nm-aist.ac.tz

Authors

Thomas Kivevele − *Department of Materials, and Energy Sciences and Engineering and African Center of Excellence for Water Infrastructure and Sustainable Energy Futures (WISE-Futures), The Nelson Mandela African Institution of Science and Technology, Arusha 23000, Tanzania*

Xiao Huang − *Department of Mechanical and Aerospace Engineering, Carleton University, Ottawa, Ontario K1S 5B6, Canada*

Complete contact information is available at:
https://pubs.acs.org/10.1021/acsomega.0c06318

Notes

The authors declare no competing financial interest.

■ REFERENCES

(1) Wang, C.; Jin, H.; Feng, H.; Wei, W.; Cao, C.; Cao, W. Study on gasification mechanism of biomass waste in supercritical water based on product distribution. *Int. J. Hydrogen Energy* **2020**, *45*, 28051.

(2) Reddy, S. N.; Nanda, S.; Dalai, A. K.; Kozinski, J. A. Supercritical water gasification of biomass for hydrogen production. *Int. J. Hydrogen Energy* **2014**, *39*, 6912−6926.

(3) Pinto, F.; Gominho, J.; André, R. N.; Gonçalves, D.; Miranda, M.; Varela, F.; Neves, D.; Santos, J.; Lourenço, A.; Pereira, H. Effect of Rice Husk Torrefaction on Syngas Production and Quality. *Energy Fuels* **2017**, *31*, 5183−5192.

(4) Singh, P.; Singh, R. K.; Gokul, P. V.; Hasan, S.-U.; Sawarkar, A. N. Thermal degradation and pyrolysis kinetics of two Indian rice husk varieties using thermogravimetric analysis. *Energy Sources, Part A Recovery, Util. Environ. Eff.* **2020**, 1−12.

(5) Alvarez, J.; Lopez, G.; Amutio, M.; Bilbao, J.; Olazar, M. Upgrading the rice husk char obtained by flash pyrolysis for the production of amorphous silica and high quality activated carbon. *Bioresour. Technol.* **2014**, *170*, 132−137.

(6) Vieira, F. R.; Romero Luna, C. M.; Arce, G. L. A. F.; Ávila, I. Optimization of slow pyrolysis process parameters using a fixed bed reactor for biochar yield from rice husk. *Biomass Bioenergy* **2020**, *132*, 105412.

(7) Adam, F.; Appaturi, J. N.; Iqbal, A. The utilization of rice husk silica as a catalyst: review and recent progress. *Catal. Today* **2012**, *190*, 2−14.

(8) Olupot, P. W.; Candia, A.; Menya, E.; Walozi, R. Characterization of rice husk varieties in Uganda for biofuels and their techno-economic feasibility in gasification. *Chem. Eng. Res. Des.* **2016**, *107*, 63−72.

(9) Bakari, R.; Kivevele, T.; Huang, X.; Jande, Y. A. C. Simulation and optimisation of the pyrolysis of rice husk: Preliminary assessment for gasification applications. *J. Anal. Appl. Pyrolysis* **2020**, *150*, 104891.

(10) Matsumura, Y.; Minowa, T.; Potic, B.; Kersten, S.; Prins, W.; Vanswaaij, W.; Vandebeld, B.; Elliott, D.; Neuenschwander, G.; Kruse, A.; Jerry Antal, M., Jr Biomass gasification in near- and super-critical water: Status and prospects. *Biomass Bioenergy* **2005**, *29*, 269−292.

(11) Kruse, A.; Gawlik, A. Biomass Conversion in Water at 330−410 °C and 30−50 MPa. Identification of Key Compounds for Indicating Different Chemical Reaction Pathways. *Ind. Eng. Chem. Res.* **2003**, *42*, 267−279.

(12) Hosseini, S. E.; Abdul Wahid, M.; Jamil, M. M.; Azli, A. A. M.; Misbah, M. F. A review on biomass-based hydrogen production for renewable energy supply. *Int. J. Energy Res.* **2015**, *39*, 1597−1615.

(13) Okolie, J. A.; Rana, R.; Nanda, S.; Dalai, A. K.; Kozinski, J. A. Supercritical water gasification of biomass: a state-of-the-art review of process parameters, reaction mechanisms and catalysis. *Sustainable Energy Fuels* **2019**, *3*, 578−598.

(14) Osada, M.; Sato, O.; Watanabe, M.; Arai, K.; Shirai, M. Water Density Effect on Lignin Gasification over Supported Noble Metal Catalysts in Supercritical Water. *Energy Fuels* **2006**, *20*, 930−935.

(15) Williams, P. T.; Onwudili, J. Composition of Products from the Supercritical Water Gasification of Glucose: A Model Biomass Compound. *Ind. Eng. Chem. Res.* **2005**, *44*, 8739−8749.

(16) Guan, Y.; Pei, A.; Guo, L. Hydrogen production by catalytic gasification of cellulose in supercritical water. *Front. Chem. Eng. China* **2008**, *2*, 176−180.

(17) Minowa, T.; Zhen, F.; Ogi, T. Cellulose decomposition in hot-compressed water with alkali or nickel catalyst. *J. Supercrit. Fluids* **1998**, *13*, 253−259.

(18) Huang, J.; Lian, X.; Wang, L.; Zhu, C.; Jin, H.; Wang, R. Hydrogen production from glucose by supercritical water gasification with Ni/Zr(Ce,Y)O2-δ catalysts. *Int. J. Hydrogen Energy* **2017**, *42*, 4613−4625.

(19) Sato, T.; Furusawa, T.; Ishiyama, Y.; Sugito, H.; Miura, Y.; Sato, M.; Suzuki, N.; Itoh, N. Effect of Water Density on the Gasification of Lignin with Magnesium Oxide Supported Nickel Catalysts in Supercritical Water. *Ind. Eng. Chem. Res.* **2006**, *45*, 615−622.

(20) Meier, D.; Ante, R.; Faix, O. Catalytic hydropyrolysis of lignin: Influence of reaction conditions on the formation and composition of liquid products. *Bioresour. Technol.* **1992**, *40*, 171−177.

(21) Kabyemela, B. M.; Adschiri, T.; Malaluan, R. M.; Arai, K. Glucose and Fructose Decomposition in Subcritical and Supercritical Water: Detailed Reaction Pathway, Mechanisms, and Kinetics. *Ind. Eng. Chem. Res.* **1999**, *38*, 2888−2895.

(22) Nanda, S.; Reddy, S. N.; Hunter, H. N.; Dalai, A. K.; Kozinski, J. A. Supercritical water gasification of fructose as a model compound for waste fruits and vegetables. *J. Supercrit. Fluids* **2015**, *104*, 112−121.

(23) Bühler, W.; Dinjus, E.; Ederer, H. J.; Kruse, A.; Mas, C. Ionic reactions and pyrolysis of glycerol as competing reaction pathways in near- and supercritical water. *J. Supercrit. Fluids* **2002**, *22*, 37−53.

(24) Guo, S.; Guo, L.; Cao, C.; Yin, J.; Lu, Y.; Zhang, X. Hydrogen production from glycerol by supercritical water gasification in a continuous flow tubular reactor. *Int. J. Hydrogen Energy* **2012**, *37*, 5559−5568.

(25) Rodriguez Correa, C.; Kruse, A. Supercritical water gasification of biomass for hydrogen production − Review. *J. Supercrit. Fluids* **2018**, *133*, 573−590.

(26) Cao, W.; Guo, L.; Yan, X.; Zhang, D.; Yao, X. Assessment of sugarcane bagasse gasification in supercritical water for hydrogen production. *Int. J. Hydrogen Energy* **2018**, *43*, 13711−13719.

(27) Kumar, A.; Reddy, S. N. In Situ Sub- and Supercritical Water Gasification of Nano-Nickel (Ni2+) Impregnated Biomass for H2 Production. *Ind. Eng. Chem. Res.* **2019**, *58*, 4780−4793.

(28) Chen, J.; Fan, Y.; Zhao, X.; E, J.; Xu, W.; Zhang, F.; Liao, G.; Leng, E.; Liu, S. Experimental investigation on gasification characteristic of food waste using supercritical water for combustible gas production: Exploring the way to complete gasification. *Fuel* **2020**, *263*, 116735.

(29) Borges, A. C. P.; Onwudili, J. A.; Andrade, H. M. C.; Alves, C. T.; Ingram, A.; Vieira de Melo, S. A. B.; Torres, E. A. Catalytic supercritical water gasification of eucalyptus wood chips in a batch reactor. *Fuel* **2019**, *255*, 115804.

(30) Sun, J.; Xu, L.; Dong, G.-h.; Nanda, S.; Li, H.; Fang, Z.; Kozinski, J. A.; Dalai, A. K. Subcritical water gasification of lignocellulosic wastes for hydrogen production with Co modified Ni/Al2O3 catalysts. *J. Supercrit. Fluids* **2020**, *162*, 104863.

(31) Basu, P.; Mettanant, V.; Leon, M. Gasification of rice husk in supercritical water In *Proceedings of the 8th World Conference on Chemical Engineering*; Association for Computing Machinery, 2009; p 520.

(32) Ferreira-Pinto, L.; Silva Parizi, M. P.; Carvalho de Araújo, P. C.; Zanette, A. F.; Cardozo-Filho, L. Experimental basic factors in the production of H2 via supercritical water gasification. *Int. J. Hydrogen Energy* **2019**, *44*, 25365−25383.

(33) Czitrom, V. One-Factor-at-a-Time versus Designed Experiments. *J. Am. Stat.* **1999**, *53*, 126−131.

(34) Yang, F.; Hanna, M. A.; Marx, D. B.; Sun, R. Optimization of hydrogen production from supercritical water gasification of crude glycerol—byproduct of biodiesel production. *Int. J. Energy Res.* **2013**, *37*, 1600−1609.

(35) Samiee-Zafarghandi, R.; Karimi-Sabet, J.; Abdoli, M. A.; Karbassi, A. Supercritical water gasification of microalga Chlorella PTCC 6010 for hydrogen production: Box-Behnken optimization and evaluating catalytic effect of MnO2/SiO2 and NiO/SiO2. *Renewable Energy* **2018**, *126*, 189−201.

(36) Kang, K.; Azargohar, R.; Dalai, A. K.; Wang, H. Noncatalytic Gasification of Lignin in Supercritical Water Using a Batch Reactor for Hydrogen Production: An Experimental and Modeling Study. *Energy Fuels* **2015**, *29*, 1776−1784.

(37) Lu, Y.; Guo, L.; Zhang, X.; Ji, C. Hydrogen production by supercritical water gasification of biomass: Explore the way to maximum hydrogen yield and high carbon gasification efficiency. *Int. J. Hydrogen Energy* **2012**, *37*, 3177−3185.

(38) Mohamed, O. A.; Masood, S. H.; Bhowmik, J. L. Optimization of fused deposition modeling process parameters for dimensional accuracy using I-optimality criterion. *Measurement* **2016**, *81*, 174−196.

(39) Ranade, S. S.; Thiagarajan, P. Selection of a design for response surface. *IOP Conf. Ser.: Mater. Sci. Eng.* **2017**, *263*, 022043.

(40) Fermoso, J.; Gil, M. V.; Arias, B.; Plaza, M. G.; Pevida, C.; Pis, J. J.; Rubiera, F. Application of response surface methodology to assess the combined effect of operating variables on high-pressure coal gasification for H2-rich gas production. *Int. J. Hydrogen Energy* **2010**, *35*, 1191−1204.

(41) Gangadharan, D.; Sivaramakrishnan, S.; Nampoothiri, K. M.; Sukumaran, R. K.; Pandey, A. Response surface methodology for the optimization of alpha amylase production by Bacillus amyloliquefaciens. *Bioresour. Technol.* **2008**, *99*, 4597−4602.

(42) Arafat Hossain, M.; Ganesan, P.; Jewaratnam, J.; Chinna, K. Optimization of process parameters for microwave pyrolysis of oil palm fiber (OPF) for hydrogen and biochar production. *Energy Convers. Manage.* **2017**, *133*, 349−362.

(43) Promdej, C.; Matsumura, Y. Temperature Effect on Hydrothermal Decomposition of Glucose in Sub- And Supercritical Water. *Ind. Eng. Chem. Res.* **2011**, *50*, 8492−8497.

(44) Su, W.; Cai, C.; Liu, P.; Lin, W.; Liang, B.; Zhang, H.; Ma, Z.; Ma, H.; Xing, Y.; Liu, W. Supercritical water gasification of food waste: Effect of parameters on hydrogen production. *Int. J. Hydrogen Energy* **2020**, *45*, 14744−14755.

(45) Hantoko, D.; Antoni; Kanchanatip, E.; Yan, M.; Weng, Z.; Gao, Z.; Zhong, Y. Assessment of sewage sludge gasification in supercritical water for H2-rich syngas production. *Process Saf. Environ. Prot.* **2019**, *131*, 63−72.

(46) Su, X.; Jin, H.; Guo, L.; Guo, S.; Ge, Z. Experimental study on Zhundong coal gasification in supercritical water with a quartz reactor: Reaction kinetics and pathway. *Int. J. Hydrogen Energy* **2015**, *40*, 7424−7432.

(47) Susanti, R. F.; Dianningrum, L. W.; Yum, T.; Kim, Y.; Lee, B. G.; Kim, J. High-yield hydrogen production from glucose by supercritical water gasification without added catalyst. *Int. J. Hydrogen Energy* **2012**, *37*, 11677−11690.

(48) Su, H.; Kanchanatip, E.; Wang, D.; Zheng, R.; Huang, Z.; Chen, Y.; Mubeen, I.; Yan, M. Production of H2-rich syngas from gasification of unsorted food waste in supercritical water. *Waste Manag.* **2020**, *102*, 520−527.

(49) Adar, E.; Ince, M.; Bilgili, M. S. Supercritical water gasification of sewage sludge by continuous flow tubular reactor: A pilot scale study. *Chem. Eng. J.* **2020**, *391*, 123499.

(50) Müller, J. B.; Vogel, F. Tar and coke formation during hydrothermal processing of glycerol and glucose. Influence of temperature, residence time and feed concentration. *J. Supercrit. Fluids* **2012**, *70*, 126−136.

(51) Wang, C.; Zhu, C.; Huang, J.; Li, L.; Jin, H. Enhancement of depolymerization slag gasification in supercritical water and its gasification performance in fluidized bed reactor. *Renewable Energy* **2021**, *168*, 829−837.

(52) Lu, Y.; Guo, L.; Zhang, X.; Yan, Q. Thermodynamic modeling and analysis of biomass gasification for hydrogen production in supercritical water. *Chem. Eng. J.* **2007**, *131*, 233−244.

(53) Basu, P.; Mettanant, V., Biomass Gasification in Supercritical Water—A Review. *International Journal of Chemical Reactor Engineering*; Academic press, 2009; Vol 7.

(54) Yan, M.; Su, H.; Zhou, Z.; Hantoko, D.; Liu, J.; Wang, J.; Wang, R.; Kanchanatip, E. Gasification of effluent from food waste treatment process in sub- and supercritical water: H2-rich syngas production and pollutants management. *Sci. Total Environ.* **2020**, *730*, 138517.

(55) Susanti, R. F.; Veriansyah, B.; Kim, J.-D.; Kim, J.; Lee, Y.-W. Continuous supercritical water gasification of isooctane: A promising reactor design. *Int. J. Hydrogen Energy* **2010**, *35*, 1957−1970.

(56) Chuntanapum, A.; Matsumura, Y. Char Formation Mechanism in Supercritical Water Gasification Process: A Study of Model Compounds. *Ind. Eng. Chem. Res.* **2010**, *49*, 4055−4062.

(57) Pettersson, L.; Westerholm, R. State of the art of multi-fuel reformers for fuel cell vehicles: problem identification and research needs. *Int. J. Hydrogen Energy* **2001**, *26*, 243−264.

(58) Snoeck, J.-W.; Froment, G. F.; Fowles, M. Steam/CO2 Reforming of Methane. Carbon Formation and Gasification on Catalysts with Various Potassium Contents. *Ind. Eng. Chem. Res.* **2002**, *41*, 3548−3556.

(59) Wang, C.; Zhu, C.; Cao, W.; Wei, W.; Jin, H. Catalytic mechanism study on the gasification of depolymerizing slag in supercritical water for hydrogen production. *Int. J. Hydrogen Energy* **2021**, *46*, 2917−2926.

(60) Gratuito, M. K. B.; Panyathanmaporn, T.; Chumnanklang, R.-A.; Sirinuntawittaya, N.; Dutta, A. Production of activated carbon from coconut shell: Optimization using response surface methodology. *Bioresour. Technol.* **2008**, *99*, 4887−4895.

(61) Behera, S. K.; Meena, H.; Chakraborty, S.; Meikap, B. C. Application of response surface methodology (RSM) for optimization of leaching parameters for ash reduction from low-grade coal. *Int. J. Min. Sci. Technol.* **2018**, *28*, 621−629.